UNIVERSITY OF GAZİANTEP
GRADUATE SCHOOL OF
NATURAL & APPLIED SCIENCES

EFFECT OF AGGREGATE SIZE AND AMOUNT ON THE MECHANICAL PROPERTIES OF ENGINEERED CEMENTITIOUS COMPOSITES INCORPORATING FLY ASH AND SLAG

M. Sc. THESIS
IN
CIVIL ENGINEERING

BY
MEHMET TURHAN ARIK
JANUARY 2011

Effect of Aggregate Size and Amount on the Mechanical Properties of Engineered Cementitious Composites Incorporating Fly Ash and Slag

M.Sc. Thesis
in
Civil Engineering
University of Gaziantep

Supervisor
Assoc. Prof. Dr. Mustafa ŞAHMARAN

by
Mehmet Turhan ARIK
January 2011

T.C.
UNIVERSITY OF GAZİANTEP
GRADUATE SCHOOL OF
NATURAL & APPLIED SCIENCES
CIVIL ENGINEERING DEPARTMENT

Name of the thesis:	Effect of Aggregate Size and Amount on the Mechanical Properties of Engineered Cementitious Composites Incorporating Fly Ash and Slag
Name of the student:	Mehmet Turhan ARIK
Exam date:	January 31, 2011

Approval of the Graduate School of Natural and Applied Sciences

Prof. Dr. Ramazan KOÇ
Director

I certify that this thesis satisfies all the requirements as a thesis for the degree of Master of Science.

Assoc. Prof. Dr. Mustafa GÜNAL
Head of Department

This is to certify that we have read this thesis and that in our opinion it is fully adequate, in scope and quality, as a thesis for the degree of Master of Science.

Assoc. Prof. Dr. Mustafa ŞAHMARAN
Supervisor

Examining Committee Members	Signature
Prof. Dr. Mustafa ÖZAKÇA	
Assoc. Prof. Dr. İ. Özgür YAMAN	
Assoc. Prof. Dr. Mustafa ŞAHMARAN	

ABSTRACT

EFFECT OF AGGREGATE SIZE AND AMOUNT ON THE MECHANICAL PROPERTIES OF ENGINEERED CEMENTITIOUS COMPOSITES INCORPORATING FLY ASH AND SLAG

ARIK, Mehmet Turhan
M.Sc. in Civil Engineering
Supervisor: Assoc. Prof. Dr. Mustafa ŞAHMARAN
January 2011, 81 pages

Engineered Cementitious Composites (ECC) is a special type of high performance fiber reinforced cementitious composite featuring high ductility and damage tolerance under mechanical loading, including tensile and shear loadings. The relative high cost remains an obstacle for wider commercial use of ECC. The replacement of Portland cement by fly ash and slag, and an increase in the amount and size of aggregate used in ECC production can lower its cost and enhance its greenness of composites, since the production of these materials needs less energy and causes less carbon dioxide emission than cement. The studies reported in this thesis indicate that an experimental program is undertaken to study the dependence of the composite properties on its mixture composition governed by mineral admixture types and amount, and maximum aggregate size and amount. Test results revealed that with proper selection of the type and amount of mineral admixture, aggregates within the amount and size range studied do not negatively influence the ductility of ECC, increase in the age of restrained shrinkage cracking, and a significant decrease in the drying shrinkage capacity. Together with the enhanced composite mechanical properties with the standard ECC mixture produced with micro silica sand and dimensional stability enhancement, the substantial use of these mineral admixtures from industrial processes and the increasing of maximum grain size and amount of sand in the production of ECC is an important step toward sustainability in the construction industry.

Key Words: ECC (Engineered Cementitious Composites);Aggregate Size; Aggregate Amount;Mineral Admixture;Mechanical Properties;Dimensional Stability.

ÖZET

AGREGA BOYUTU VE ORANININ UÇUCU KÜL VE CÜRUF İÇEREN TASARLANMIŞ ÇİMENTO ESASLI KOMPOZİTLERİN MEKANİK ÖZELLİKLERİ ÜZERİNE ETKİLERİ

ARIK, Mehmet Turhan
Yüksek Lisans Tezi, İnşaat Mühendisliği Bölümü
Tez Yöneticisi: Doç. Dr. Mustafa ŞAHMARAN
Ocak 2011, 81 sayfa

Tasarlanmış Çimento Esaslı Kompozit (ECC), yüksek performanslı lif donatılı çimento esaslı kompozitlerin özel bir çeşidi olup, çekme ve kayma yüklemeleri gibi mekanik yükler altında sünek ve hasara karşı toleranslı bir davranış sergilemektedir. ECC'nin geniş ticari alanlarda kullanılmasının önündeki en önemli engel yüksek maliyetidir. ECC üretiminde Portland çimentosunun bir kısmının uçucu kül veya cüruf ile yer değiştirilmesi ve kullanılmakta olan agrega boyut ve miktarının arttırılması ile, ECC'nin maliyeti azaltılıp çevreye duyarlılığı arttırılabilir. Çünkü bu malzemelerin üretiminde daha az enerjiye ihtiyaç bulunulup üretimleri esnasında çok daha az karbondioksit salınımı gerçekleşmektedir. Bu tezde mineral katkı çeşidi (uçucu kül veya cüruf) ve miktarı, en büyük agrega tane büyüklüğü ve agrega kullanım oranı gibi, karışım paremetrelerinin ECC kompozitinin özellikleri üzerindeki etkileri çalışılmıştır. Test sonuçları, uygun mineral katkı çeşidi ve miktarının kullanılması ile, deneysel çalışmalar kapsamında kullanılan agrega miktarı ve boyutunun arttırılarak üretilen ECC'nin süneklilik özelliği olumsuz biçimde etkilenmeden kısıtlanmış rötre çatlak yaşının geciktirilip kuruma rötre kapasitesinin azaltılabileceğini göstermiştir. Önemli ölçüde endüstriyel atık katkılarının kullanımı ve agrega miktarı ve boyutunun arttırılması ile üretilen ECC karışımlarından, mikro silis kumu ile üretilen standart ECC karışımına oranla daha iyi mekanik performansın elde edilmesine ilaveten bu şekilde geliştirilmiş olan kompozit sürdürülebilir yapı endüstrisine yönelik önemli bir adım sayılabilir.

Anahtar kelimeler: Tasarlanmış Çimento Esaslı Kompozit (ECC), agrega boyutu, agrega miktarı, mineral katkı, mekanik özellikler, boyutsal stabilite.

ACKNOWLEDGEMENT

This dissertation has been completed under the guidance of my advisor, Assoc. Prof. Dr. Mustafa ŞAHMARAN. Without his support, inspiration, dedication of time and energy throughout the past year, I could have never completed this work. I owe forever my sincerest gratitude to him, for opening my eyes to the innovative material technology world, and for challenging me with novel research ideas capable of solving real-world problems.

I must acknowledge the financial assistance of the Scientific and Technical Council of Turkey (TÜBİTAK) provided under Project: MAG-108M495.

My deep appreciations and thanks to Research Asistant Hasan Erhan YÜCEL and Serhat DEMİRHAN for his helps and valuable suggestions.

I would also like to special thanks to Prof. Dr. Mustafa ÖZAKÇA, Assoc. Prof. Dr. İ. Özgür YAMAN for serving on the committee.

Thanks are also due to Şerife KIDIR the woman who illuminated my path and inspired me throughout my life.

Finally, I would also thanks to my family for their support and encouragement during my study.

CONTENTS

Page

LIST OF FIGURES

LIST OF TABLES

LIST OF SYMBOLS/ABBREVIATIONS

ASR	Alkali silica reaction
AWR	Aggregate wear index
C	Portland cement
CSH	Calcium silica hydrate
CW	Microcracks width
$e^{f\phi}$	Accounts for the changes in bridging force for fibers crossing at an inclined angle to the crack plane
ECC	Engineered cementitious composites
ESEM	Environmental scanning electron microscope
f	Snubbing coefficient
$f\left(\frac{a}{W}\right)$	Geometric calibration factor
FA	Fly ash
FRC	Fiber reinforced concrete
HPFRCC	High performance fiber reinforced cementitious composites
HRWR	High range water reducing admixture
HVFA	High volume fly ash
J'_b	Complimentary energy
J_{tip}	Fracture energy of the mortar matrix
K_m	Fracture toughness of the mortar matrix
L_f	Fiber length
LVDT	Linear variable displacement transducer
MAS	Maximum aggregate size
MIP	Mercury intrusion porosimetry
P_Q	Applied load
P(δ)	Pullout load versus displacement relation of a single fiber aligned normal to the crack plane
p(ϕ)	Probability density functions of the fiber orientation angle
PVA	Poly-vinyl-alcohol
p(z)	Centroidal distance from the crack plane
R/C	Reinforced concrete
R/ECC	Reinforced ECC
RH	Relative humidity
S	Slag
SEM	Scanning electron microscopy
V_f	Fiber volume fraction
W/C	Water to cement ratio
z	Centroidal distance of a fiber from the crack plane
σ_0	Maximum crack bridging stress
σ_{fc}	First cracking strength of the mortar matrix
δ_0	Crack opening
ϕ	Orientation angle of the fiber

CHAPTER I

INTRODUCTION

1.1 General

Concrete is a brittle material that exhibits failure arising from the extensional deformation at the location of first cracking after the peak load. Therefore, while the stress exceeds the tensile strength of concrete, a single crack forms and the crack width easily achieves a visible propagation. Since cracking in structures reduces the load-carrying capacity, and allows other chemical agents, for overcoming this disadvantage, recently many attempts have been done. To effectively solve this severe problem, a new type of composite, called as Engineered Cementitious Composites (ECC), reducing the brittle behavior of concrete has been developed in last decades. ECC is a special type of high performance fiber-reinforced cementitious composite featuring high ductility and damage tolerance under mechanical loading, including tensile and shear (Li, 1997; Li et al., 2001; Li, 2003) loadings. By employing micromechanics-based material optimization (Li, 1997; Lin and Li, 1997), tensile strain capacity in excess of 3% under uniaxial tensile loading can be attained with only 2% fiber content by volume (Li, 1997; Lin et al., 1999). The characteristic strain-hardening after matrix first cracking is accompanied by sequential development of multiple microcracking and the tensile strain capacity is 300-500 times greater than that of normal concrete. Even at ultimate load, the crack width remains on the order of 50 to 80 micrometer. This tight crack width is self-controlled and, whether the composite is used in combination with conventional reinforcement or not, it is a material characteristic independent of rebar reinforcement ratio. In contrast, normal concrete and fiber-reinforced concrete rely on steel reinforcement for crack width control. The tight crack width of ECC is important to the durability of ECC structures as the tensile ductility is to the structural safety at ultimate limit state. These properties, together with a relative ease of production including self-consolidation casting (Kong et al., 2003a; Kong et al., 2003b) and shotcreting (Kim et al., 2003), make them suitable for

various civil engineering applications. ECC is currently emerging in full scale structural applications (Li et al., 2005; Kunieda and Rokugo, 2006). The ingredients and mix proportions of ECC are optimized through micromechanics-based material design theory to satisfy strength and energy criteria to attain high composite tensile ductility (Li, 1997; Li et al., 2001; Li, 2003; Yang and Li, 2006). The type, size and amount of fiber, matrix ingredients and interface characteristics are tailored for multiple cracking and controlled crack width in ECCs. Aggregates typically occupy an important volume fraction in conventional concrete, and thus have important effects on different aspects of material properties. In addition to their role as an economic filler, aggregates help to control dimensional stability of cement-based materials, which may be considered to consist of a framework of cement paste with relatively large shrinkage movements restrained by aggregates. However, high aggregate content and presence of coarse aggregates in a paste tends to increase the tortuosity of the fracture path, and lead to a tough matrix which delays crack initiation and prevents steady-state flat-crack propagation in ECC, resulting in loss of tensile ductility. Moreover, the introduction of aggregates with a particle size larger than the average fiber spacing leads to balling and greater interaction of fibers between the large aggregate particles, and the effect becomes more pronounced as the volume and the maximum size of aggregate particles increase. Therefore, an increase in aggregate size makes it more difficult to achieve a uniform dispersion of fibers. The greater the volume and size of aggregates, the more clumping and interaction of fibers would occur. Therefore, the amount and size of the aggregates is expected to have a significant influence on the properties of composite. Hence, in spite of positive effects of aggregates on dimensional stability and economy of fiber reinforced cement composites, there are limits on aggregate size and volume content beyond which problems with fiber dispersability, fresh mix workability and matrix toughness may start to damage the composite material performance characteristics. Therefore, instead of coarse aggregate, standard ECC incorporates fine aggregate with an aggregate to binder ratio (A/B) of 0.36 to maintain adequate stiffness and volume stability (Li et al., 1995). The binder system is defined as the total amount of cementitious material, i.e. cement and mineral admixture, generally fly ash, in ECC. The silica sand has a maximum grain size of 250 μm and a mean size of 110 μm. Another purpose of using fine silica sand is to obtain the optimum gradation of particles to produce good workability (Fischer and Li, 2003).

Due to environmental and economical reasons, there is a growing trend to use industrial wastes or by-products as supplementary materials or admixtures in the production of cementitious composite. Among the various suppelementary materials, fly ash and slag are the most commonly available mineral admixtures. Because of several potential benefits, fly ash and slag have increasingly found use in high performance concrete in the last few decades (Berry and Malhotra, 1980; Mehta, 1985; Read et al., 1990; Swamy and Ammar, 1990; Malhotra, 1993). Increase in long-term compressive strength (Malhotra, 1980; Naik and Ramme, 1990; Sivasundaram et al., 1990), decrease in shrinkage (Hogan and Meusel, 1981; Tikalsky et al., 1988; Şahmaran et al., 2007; Şahmaran et al., 2009) and decrease in chloride ion penetration (Rose 1987; Haque et al., 1992) have been achieved through proper selection of the type of fly ash, slag and mix proportions.

In the past few decades, substitution of mineral admixtures, such as fly ash (FA) and slag (S), has been of great interest and gradually applied to practical applications of ECC (Kim et al., 2004; Kim et al., 2007; Wang and Li, 2007; Young et al., 2007; Zhou et al., 2009). Fly ash is a by product of the coal power plant, whereas slag is a by product in the manufacture of pig iron. Both of these waste materials from industrial processes are usually available in large quantities and at a fraction of the price of cement. The absence of coarse aggregate in ECC results in a higher cement content. Partial replacement using fly ash or slag reduces the environmental burden. Further, it has been found that incorporating high amount of FA, especially Class-F fly ash, can reduce the matrix toughness and improve the robustness of ECC in terms of tensile ductility. Additionally, unhydrated fly ash particles with small particle size and smooth spherical shape serve as filler particles resulting in higher compactness of the fiber/matrix interface transition zone that leads to a higher frictional bonding. This aids in reducing the steady-state crack width beneficial for long-term durability (Lepech and Li, 2005a; Lepech and Li, 2005b; Wang and Li, 2007; Young et al., 2007) of the structure. Since the increase in aggregate size and amount leads to an increase in the matrix toughness, locally available aggregate could successfully be used in conjunction with high volume mineral admixture in the production of ECC. No information is currently available on the influence of aggregate size and amount on the performance (ductility, mechanical behavior and dimensional stability) of ECC. Accordingly, the main objective of the current research is to design a new class

of ECCs with a matrix incorporating locally available aggregates that can show similar tensile properties to standard ECC mixtures containing micro-silica sand.

1.2 Research Objectives and Scope

An experimental program is undertaken to study the dependence of the ECC composite properties on its mix composition governed by mineral admixture types and amount, and maximum aggregate size and aggregate/binder ratios. The focus with regard to this material has been on achieving moderately high compressive strength, high dimensional stability, improved elastic modulus and more environmental friendly, while maintaining superior ductility, represented by strain-hardening behavior. ECC mixtures contain mineral admixture (fly ash or slag) with mineral admixture/cement ratio of 1.2 or 2.2, fine aggregate with maximum sizes of 0.4 or 1.0 mm and aggregate/binder ratios of 0.36, 0.45 and 0.55. Within the objective of this experimental study, 24 mixtures of ECC were prepared (12 mixtures for each of fly ash and slag) keeping water-to-cementitious materials ratio constant at 0.27. In the material development, micromechanics was adopted to properly select ECC composition based on micromechanical studies on matrix (ECC without PVA fiber) properties. The influences of investigated parameters on the composite properties including the compressive and flexural strength, ductility and shape of the load-displacement curves were supported by microstructural studies of the cement paste-aggregate interface and fracture surfaces. Microstructural studies were used based on the scanning electron microscope (SEM) observations and Mercury Intrusion Porosimetry tests (MIP). In addition, dimensional stability characteristics, drying shrinkage and shrinkage cracking potential, of ECC specimens were investigated. For each concrete mixture the potential for restrained shrinkage cracking was evaluated using the ring test. As a result, this study contributes to the discussion of fly ash and slag replacement, aggregate size and amount in ECC. Together with this mechanical and dimensional stability enhancement, the substantial use of these waste materials from industrial processes is an important step toward sustainability in the construction industry.

In Chapter 2, hardened and durability properties, application of ECC, and pozzolanic materials such as fly ash and ground granulated blast furnace slag are discussed. In

Chapter 3, experimental program, materials properties and tests on mechanical properties and dimensional stability of ECC are discussed. The results of the experimental studies are presented and discussed in Chapter 4. The conclusions of the research are presented in Chapter 5.

CHAPTER II

LITERATURE REVIEW AND BACKROUND

2.1 Introduction

Increased durability of reinforced concrete structures is typically associated with a dense concrete matrix, i.e. a very compact microstructure expected to lower permeability and reduce transport of corrosives to steel reinforcing (Beeldens and Vandewalle, 2001; Oh et al., 2002). This can be achieved with a well-graded particle size distribution (Hwang, 1996), slag, fly ash and silica fume (Chang, 2001), or low w/c ratios (Mehta, 1986). These concepts, however, rely upon the concrete to remain uncracked within a structure throughout its expected lifetime and resist the transport of water, chloride ions, oxygen, etc. through its dense microstructure. In this presumed uncracked state, numerous concrete materials have shown promising durability in laboratory tests (Weiss and Shah, 2002; Mora et al., 2003).

In practice, however, reinforced concrete members crack due to both applied structural loading and shrinkage and thermal deformations, which are practically inevitable and often anticipated in restrained conditions (Wittmann, 2002; Mihashi and De Leite, 2004). These cracks provide pathways for the penetration of aggressive ions to cause concrete deterioration. Chlorides, oxygen, and carbonation agents can migrate through cracks and ultimately lead to corrosion of reinforcement. Although the uncracked concrete between adjacent cracks can be extremely dense and nearly impermeable, the presence of cracks results in a high overall permeability and unhindered access of corrosives (Bakker, 1988; Gerard et al., 1997; Hearn, 1999) to reinforcing steels through the concrete cover. Thus, at the root of this durability problem is the brittle nature of concrete materials. To solve this serious problem, a fundamental solution which reduces the brittle nature of concrete is needed.

Through the use of High Performance Fiber Reinforced Cementitious Composites (HPFRCC), which display significantly higher ductility than concrete

(R/C), durability problems resulting from cracking may be solved (Li and Stang, 2004). Yet to prove acceptable for many applications, these materials must show high ductility without forming large cracks and enhanced material and structural durability by exhibiting such characteristics as excellent protection of steel reinforcement, resistance to freeze thaw cycles, de-icing salt scaling resistance and demonstration of long term mechanical performance. The introduction of materials which provide both ductility and durability can significantly impact the design of future, more durable infrastructure systems.

2.2 Engineered Cementitious Composites (ECC)

As a new class of HPFRCC materials, Engineered Cementitious Composites (ECC) is a ductile fiber reinforced cementitious composite micromechanically designed to achieve high damage tolerance under severe loading and high durability under normal service conditions (Li, 1998; Li et al., 2001; Li, 2003). The most distinctive characteristic separating ECC from conventional concrete and fiber reinforced concrete (FRC) is an ultimate tensile strain capacity between 3% to 5%, depending on the specific ECC mixture. This strain capacity is realized through the formation of many closely spaced microcracks, allowing for a strain capacity over 300 times that of normal concrete. These cracks, which carry increasing load after formation, allow the material to exhibit strain hardening, similar to many ductile metals.

While the components of ECC may be similar to FRC, the distinctive ECC characteristic of strain hardening through microcracking is achieved through micromechanical tailoring of the components (i.e. cement, aggregate, and fibers) (Li, 1998; Lin et al., 1999; Li et al., 2001; Li, 2003), along with control of the interfacial properties between components. Fracture properties of the cementitious matrix are carefully controlled through mix proportions. Fiber properties, such as strength, modulus of elasticity, and aspect ratio have been customized for use in ECC. The interfacial properties between fiber and matrix have also been optimized in cooperation with the manufacturer for use in this material. Typical mix proportions of ECC using a poly-vinyl-alcohol (PVA) fiber are given in Table 2.1.

Table 2.1 Typical mix design of ECC material

Cement	Water	Aggregate	Fly Ash	HRWR*	Fiber (%)
1.00	0.58	0.80	1.20	0.013	2.00

*HRWR = High range water reducing admixture; all ingredients proportion by weight except for fiber.

While most HPFRCCs rely on a high fiber volume to achieve high performance, ECC uses low amounts, typically 2% by volume, of short, discontinuous fiber. This low fiber volume, along with the common components, allows flexibility in construction execution. To date, ECC materials have been engineered for self-consolidation casting (Kong et al., 2003a), extrusion (Stang and Li, 1999), shotcreting (Kim et al., 2003), and conventional mixing in a gravity mixer or conventional mixing truck (Lepech and Li, 2007).

Figure 2.1 shows a typical uniaxial tensile stress-strain curve of ECC material containing 2% poly-vinyl-alcohol (PVA) fiber (Weimann and Li, 2003). The characteristic strain-hardening behavior after first cracking is accompanied by multiple microcracking. The crack width development during inelastic straining is also shown in Figure 2.1. Even at ultimate load, the crack width remains smaller than 80 μm. This tight crack width is self-controlled and, whether the composite is used in combination with conventional reinforcement or not, it is a material characteristic independent of rebar reinforcement ratio. In contrast, normal concrete and fiber reinforced concrete rely on steel reinforcement for crack width control. Under severe bending loads, an ECC beam deforms similar to a ductile metal plate through plastic deformation (Figure 2.2). In compression, ECC materials exhibit compressive strengths similar to high strength concrete (e.g. greater than 60 MPa) (Lepech and Li, 2007).

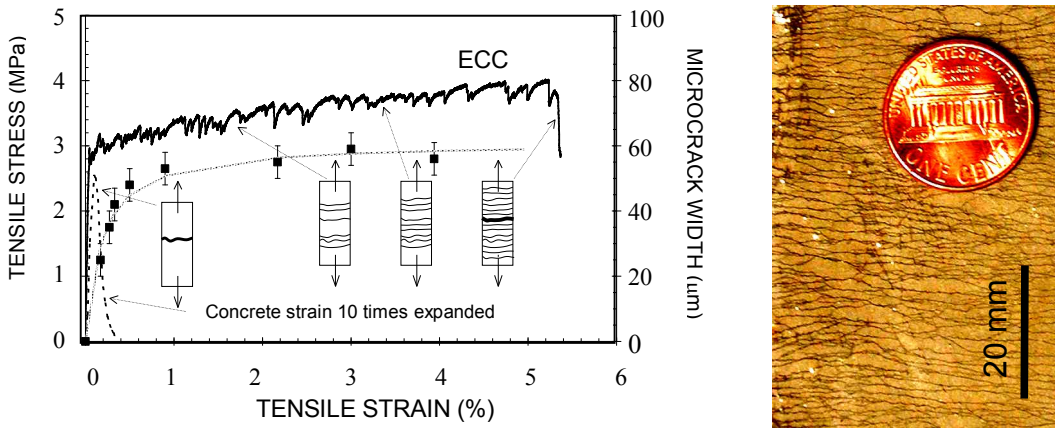

Figure 2.1 Typical tensile stress-strain curve and crack width development of ECC (Weimann and Li, 2003)

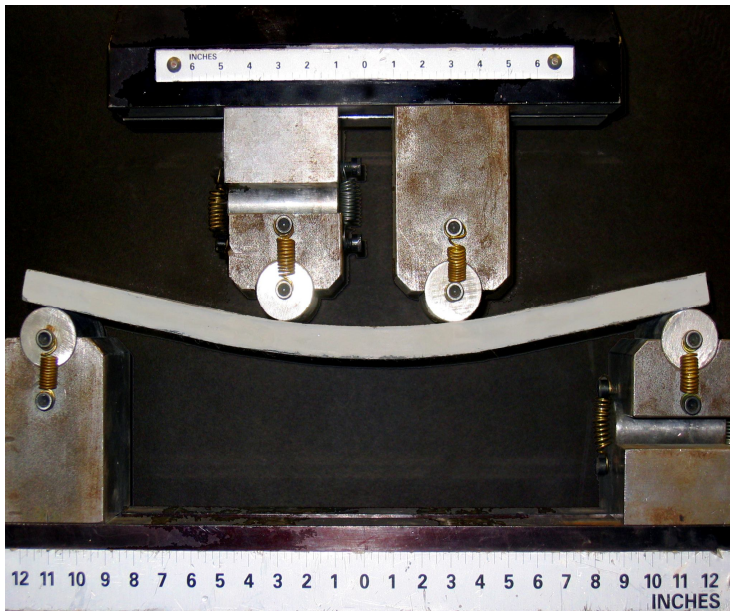

Figure 2.2 Response of ECC under flexural loading

2.3 Design of Engineered Cementitious Composites

The first priority when designing ECC material is to ensure the formation of multiple cracks and strain-hardening behavior under load. This allows large deformations to be distributed over multiple micro-cracks. The basis of multiple micro-cracking and strain hardening within ECC is the propagation of steady state cracks which were first characterized by Marshall and Cox (1988), and extended to fiber reinforced cementitious composites by Li and Leung (1992) and Lin et al. (1999). By forming steady state "flat cracks" which maintain a constant crack width while propagating,

rather than Griffith-type cracks which widen during propagation as in typical tension-softening fiber reinforced cementitious materials, ECC material exhibits multiple micro-cracks which saturate the specimen while undergoing strain-hardening during extreme tensile deformation. The formation of multiple steady state cracking is governed by the bridging stress versus crack width opening relation along with the cracking toughness of the mortar matrix. To achieve this phenomenon the inequality shown in Equation-2.1 must be satisfied.

$$J_b^{'} = \sigma_0\delta_0 - \int_0^{\delta_0}\sigma(\delta)d\delta \geq J_{tip} \approx \frac{K_m^2}{E_m} \qquad (2.1)$$

where J'_b is the complimentary energy shown in Figure 2.3, σ_0 and δ_0 are the maximum crack bridging stress and corresponding crack opening, J_{tip} is the fracture energy of the mortar matrix, K_m is the fracture toughness of the mortar matrix, and E_m is the elastic modulus of the mortar matrix. In addition to the fracture energy criterion, a strength criterion expressed in Equation-2.2 must be satisfied.

$$\sigma_0 > \sigma_{fc} \qquad (2.2)$$

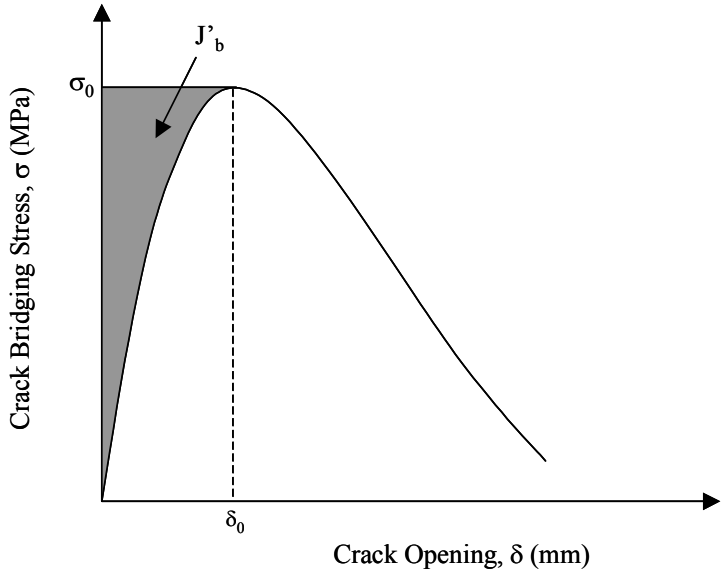

Figure 2.3 Crack bridging stress versus crack opening relation

where, σ_0 is the maximum crack bridging stress and σ_{fc} is the first cracking strength of the mortar matrix. For saturated multiple cracking, Wang and Li (2004) found that Equation-2.2 must be satisfied at each potential crack plane, where σ_{fc} is understood as the cracking stress on that crack plane.

Once an ECC mixture is selected which sufficiently meets the two above criteria, the formation of multiple steady state cracks, and strain-hardening performance, can be realized. However, in addition to forming these cracks, the material must also be designed to exhibit crack widths below the 100 μm threshold limit. This can be achieved through tailoring of the crack bridging versus crack opening relation referenced in Equation-2.1. The maximum steady state crack width exhibited during ECC multiple cracking can be assumed to be δ_0, the crack width corresponding to the maximum crack bridging stress, σ_0, as shown in Figure 2.3. If the crack width were to grow beyond δ_0, the crack bridging stress would begin to fall, in which case the crack would localize and multiple crack formation would cease. By keeping δ_0 below the 100 μm threshold, the ECC material can exhibit multiple cracking and strain hardening performance.

Lin et al. (1999) proposed the formulation of the crack bridging stress versus opening relationship based on summing the bridging force contribution of fibers that cross a given crack plane. This relation in expressed in Equation-2.3.

$$\sigma(\delta) = \frac{4V_f}{\pi d_f^2} \int_{\phi=0}^{\pi/2} \left(\int_{z=0}^{(L_f/2)\cos\phi} P(\delta) e^{f\phi} p(\phi) p(z) dz \right) d\phi \qquad (2.3)$$

where V_f is the fiber volume fraction, d_f is the fiber diameter, ϕ is the orientation angle of the fiber, L_f is the fiber length, z is the centroidal distance of a fiber from the crack plane, f is a snubbing coefficient, and $p(\phi)$ and p(z) are probability density functions of the fiber orientation angle and centroidal distance from the crack plane, respectively. $P(\delta)$ is the pullout load versus displacement relation of a single fiber aligned normal to the crack plane, also described in Lin et al. (1999). The factor $e^{f\phi}$ accounts for the changes in bridging force for fibers crossing at an inclined angle to the crack plane.

Using these basic micromechanical models to tailor the ECC material, a composite can be designed to undergo large deformations, up to several percent, without sacrificing low permeability due to large crack widths. The application of material design procedures, such as those outlined above, allow materials engineers to carefully match material characteristics to specific structural demands, such as strain capacity and low permeability.

2.4 Mechanical Properties and Durability of ECC

2.4.1 Fatigue

The performance of ECC has been investigated in high fatigue scenarios, such as rigid pavement overlay rehabilitation. In these overlay applications, reflective cracking through the new overlay is of greatest concern. Existing cracks and locally reduced load capacity in the substrate pavement can result in flexural fatigue within the overlay structure. To evaluate ECC performance as a rigid pavement overlay material, both ECC/concrete and concrete/concrete overlay specimens were tested in flexural fatigue (Zhang and Li, 2002). Test results show that the load capacity of ECC/concrete overlay specimens was double that of concrete/concrete overlay specimens, the deformability of ECC/concrete specimens was significantly higher, and the fatigue life was extended by several orders of magnitude. Further, the microcracking deformation mechanism of ECC effectively eliminated reflective cracking. Similar advantages in the fatigue resistance of ECC have also been found in comparison to polymer cement mortars (Suthiwarapirak et al., 2002). Fatigue resistance of ECC for repair of viaducts subjected to train loading was studied by Inaguma et al. (2005). In fatigue-prone concrete infrastructure, the application of ECC materials may be able to significantly lengthen service-life, reduce maintenance events, and life cycle costs.

2.4.2 Spall Resistance

Greater resistance to spalling, brought about by reinforcing steel corrosion, can be achieved through the high ductility of ECC material. It is well known that once corrosion of steel reinforcing is initiated, corrosion debris expands against the surrounding concrete, creating a tensile circumferential stress state (i.e. hoop stress)

in the cover concrete. This may lead to tensile radial cracking and subsequent spalling of the cover, resulting in a shortening of the structural service life. The spall resistance of ECC was investigated Kanda et al. (2003) and Miyazato and Hiraishi (2005) by pushing a tapered steel rod into a hole cast through an ECC slab in order to simulate the expansive force generated by a corroding rebar. The test results showed that ECC accommodated the simulated expansion by "plastic yielding" through the formation of radial microcracks, while concrete fractured in a brittle nature under the expansive force. Figure 2.4 shows the signature damage and failure modes in ECC and concrete slabs after testing. Even with identical material compressive strengths, a significantly higher load (30 kN) was sustained by the ECC slab as compared to the concrete slab (~7 kN).

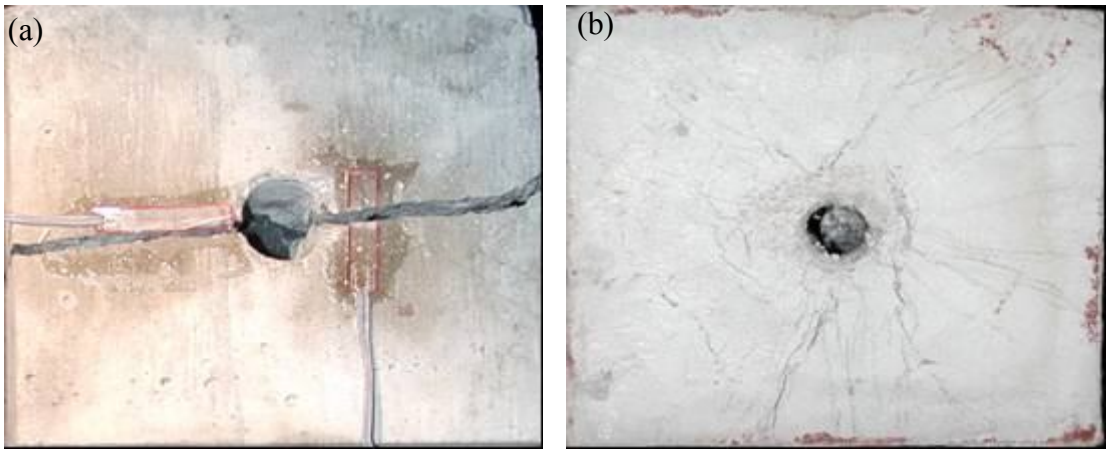

Figure 2.4 Failure modes of the slab (a) concrete, and (b) ECC

2.4.3 Wear Testing and Abrasion

For pavement surface and bridge deck repairs, ECC must provide an adequate surface for driving and braking, while withstanding traffic abrasion. Specimens were cured for 28 days and subjected to both static friction testing and wear track testing according to Michigan Test Method 111 (2001). Initial friction forces between vehicle tires operating at 65 kph and the textured ECC specimens were determined using a Michigan Department of Transportation (MDOT) static friction tester. All static friction tests were conducted on a wet pavement surface. Following initial friction testing, ECC specimens were subjected to 4 million tire passes to simulate long term tire wear. After wearing, friction forces were again determined to assess

deterioration or surface polishing during wearing. These final friction forces equate to an Aggregate Wear Index (AWI) used for long term evaluation of pavement wear. AWI values for the textured ECC samples tested range from 1.6 kN to 2.3 kN (Li et al., 2003). The established minimum AWI for Michigan trunkline road surfaces is 1.2 kN, significantly lower than all ECC surfaces tested, indicating its suitability for roadway surface repairs subject to heavy traffic volumes.

2.4.4 Transport Properties

Depending on the driving force, the transportation of liquids, gases and ions through hardened concrete can occur chiefly through three different mechanisms; permeation, absorption, or diffusion. Depending upon the conditions, transport of liquids, gases and ions may be driven by one or a combination of these three mechanisms. The main driving force behind permeation is the presence of a pressure gradient. Permeation is very important for concrete structures under water such as offshore structures or fluid retaining structures such as water tanks. Absorption, driven by capillary pore suction, is the predominant transport process when unsaturated concrete is exposed to liquids. Diffusion is the most commonly studied transport process of ions, such as chloride, which accelerates the initiation of steel corrosion in concrete. When the saturated concrete is exposed to a chloride solution, a chloride concentration gradient is created between the concrete element surface and the pore solution. In this case, diffusion will be the predominant driving mechanism of chloride transport.

2.4.4.1 Permeability

Typically, the formation of cracks increases the transport properties of concrete, allowing water, oxygen and chloride ions to easily penetrate and reach the reinforcing steel and accelerate the initiation of steel corrosion in concrete. Lepech and Li (2005) studied the water permeability of mechanically loaded ECC and reinforced mortar. In that study, both ECC and reinforced mortar specimens were tensioned to identical 1.5% deformation, resulting in a variety of crack widths and number of cracks among the various specimens. The ECC specimens revealed microcracks less than 60 μm regardless of the imposed deformation level, and the

cracked specimens exhibited nearly the same water permeability as sound concrete (Figure 2.5). In contrast, cracks larger than 150 μm were easily produced in the reinforced mortar specimens under the identical imposed uniaxial deformation. The larger crack widths resulted in significant increase in water permeability of the reinforced mortar, despite the smaller number of cracks. Further, when normalized by number of cracks within the specimen, the comparable permeability of cracked ECC with sound material becomes even more apparent (Figure 2.5).

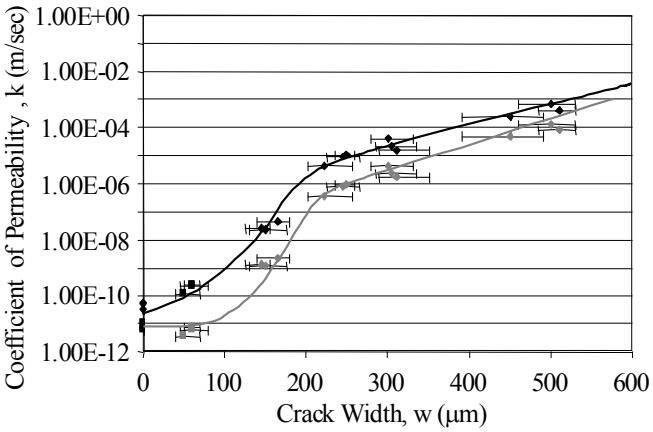

Figure 2.5 Permeability of cracked and uncracked ECC (square symbols) and reinforced mortar specimens (diamond symbols). Grey data points are permeability values normalized by number of cracks in the specimens

2.4.4.2 Diffusion

The corrosion of steel in concrete is one of the major problems with respect to the durability of reinforced concrete structures, and the penetration of chloride ions into concrete is considered to be the major cause of corrosion. Miyazato and Hiraishi (2005) was probably the first to show that the penetration depth of chloride ions into ECC cover was substantially lower than that in concrete cover, using R/C and R/ECC beams preloaded to the same level of flexural deflection and subjected to identical accelerated chloride exposure. In addition, a relation between flexural deformation levels and the effective chloride diffusion coefficient of ECC and reinforced mortar was examined by Şahmaran et al. (2007). The effective chloride diffusion was computed based on measured chloride ion concentration profiles fitted to Crank's solution to Fick's 2nd Law. Under high imposed bending deformation, the preloaded ECC beam specimens revealed multiple microcracks width (CW) less than

50 μm and an effective diffusion coefficient significantly lower than that of the similarly preloaded reinforced mortar beam because of the tight crack width control in ECC (Figure 2.6). In contrast, cracks larger than 150 μm were easily produced in reinforced mortar specimens under the same imposed deformation, producing significant increase in the effective diffusion coefficient. The effective diffusion coefficient of ECC was found to be linearly proportional to the number of cracks, whereas the effective diffusion coefficient of reinforced mortar is proportional to the square of the crack width. Therefore, the effect of crack width on chloride transport was more pronounced when compared to that of crack number. In addition, tensile performances of ECC cracked and uncracked specimens under marine environment were investigated by Li et al. (2007). Apart from the slight reductions in ultimate tensile strain and strength capacities and higher residual crack width, the test results largely confirm the durability performance of ECC material under accelerated aging, even in cases where the material experiences mechanical loading that deforms it into the strain-hardening stage prior to exposure. Healing of micro-cracks induced by the preload is evident from the recovery of elastic stiffness of the exposed pre-cracked specimens on reloading.

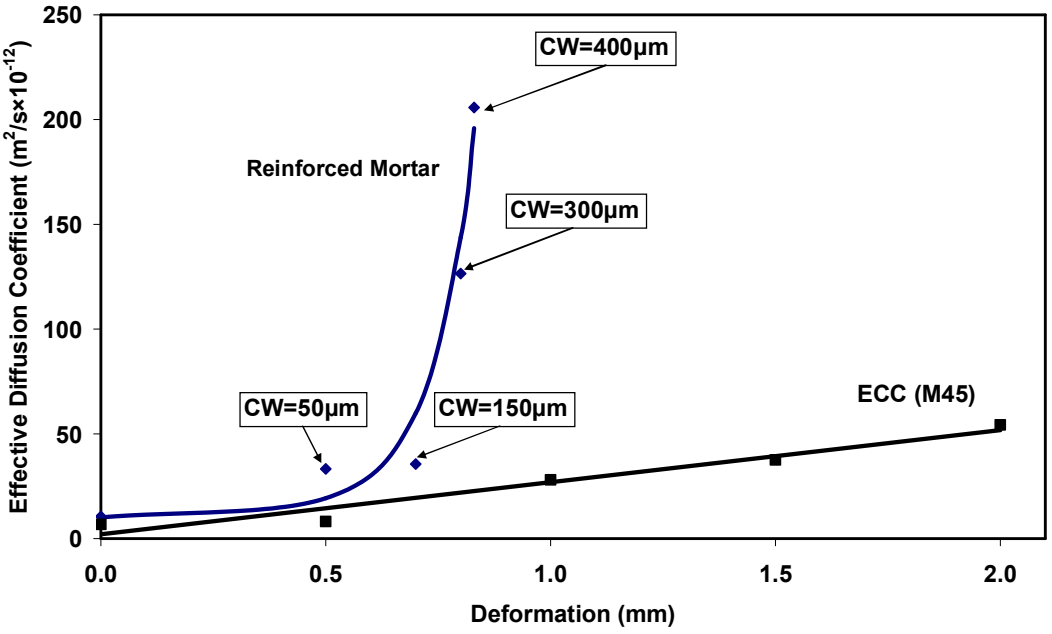

Figure 2.6 Diffusion coefficient versus pre-loading deformation level for ECC and mortar (Li et al., 2007)

2.4.4.3 Absorption

Since concrete structures in exposed conditions are generally subjected to the drying actions of wind and sun, they are rarely fully saturated when in service. Under this condition, therefore, permeability and diffusion may not be the dominant transport processes in concrete materials. Under dry or partially saturated conditions, the movement of water into concrete is controlled by capillary suction forces existing in the evacuated capillary cavities within the matrix (Martys and Ferraris, 1997). As mentioned above, cracking in ECC is fundamentally different from that which occurs in concrete or reinforced concrete. One of the concerns of ECC is its crack pattern of closely spaced cracks with tight crack width in relation to capillary suction. This concern is addressed directly in the study conducted by Şahmaran and Li (2008a) by measuring the sorptivity and absorption properties of pre-cracked ECC material. After various numbers of microcracks were introduced by mechanical loading, water absorption and sorptivity tests were performed to develop an understanding of how microcracks accelerated the deterioration process. Figure 2.7 shows the relationship between the sorptivity ($mm/min^{1/2}$) over six hours and the number of cracks, for ECC specimens. Corresponding values for virgin ECC specimens (data points with zero number of cracks) are also included in this plot. As seen from the figure, the presence of micro-cracking in ECC significantly alters the transport properties measured as a function of the number of micro-cracks. The water absorption increase is fairly high as the number of cracks on the surface of the ECC specimens increases. Therefore, the sorptivity test shows that micro-cracked ECC specimens would be more vulnerable to attack than virgin specimens. As the number of cracks along the specimen grows, the sorptivity of ECC increased exponentially. Even so, the sorptivity values of pre-loaded ECC specimens up to a strain representing 1.5% on the exposed tensile face is not particularly high when compared to that of normal concrete, probably due to higher amount of cementitious materials, lower water-cementitious materials ratio, high fly ash content and the absence of coarse aggregate. Moreover, in the same study, Şahmaran and Li (2008a) also studied the absorption rate in cracked ECC, and found that the use of water repellent admixture in the production of ECC could easily inhibit the sorptivity even for the mechanically pre-loaded ECC (Figure 2.7).

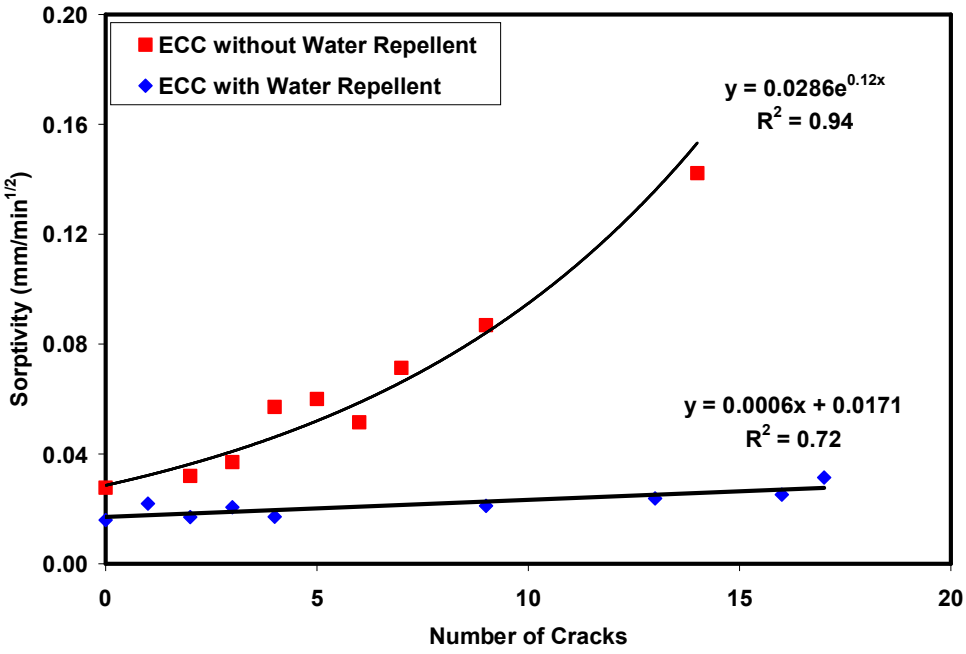

Figure 2.7 Sorptivity versus number of crack for ECC mixtures (Şahmaran and Li, 2008a)

The reason for the relatively low permeation and diffusion cracked ECC specimens are not only due to the tight crack width but also the presence of self-healing of the microcracks. The self-healing of cracks becomes prominent when crack width is small. Based on experimental results, Evardsen (1999) and Reinhardt and Jooss (2003) proposed that crack widths below 0.10 mm can be closed by a self-healing process (Evardsen, 1999; Reinhardt and Joss, 2003). In the case of precracked ECC specimens exposed to water or salt solution or under wet and dry cycles, micro-cracks in ECC were found to close due to self-healing, thus slowing further water intake, reducing the rate of water absorption and diffusion (Lepech and Li, 2005; Şahmaran et al., 2007). For example, an environmental scanning electron microscope (ESEM) observation of the fractured surface of ECC across a healed crack after exposed to salt solution is shown in Figure 2.8. The ESEM observations show that most of the products seen in the cracks were newly formed calcium-silicate-hydrate (C-S-H) gels, which are the basic cementing compound produced by the hydration reactions. This can be attributed primarily to the large fly ash content and relatively low water to binder ratio within the ECC mixture. The continued pozzolanic activity of fly ash is responsible for the self-healing of the crack which further reduces the ingress of the chloride ions.

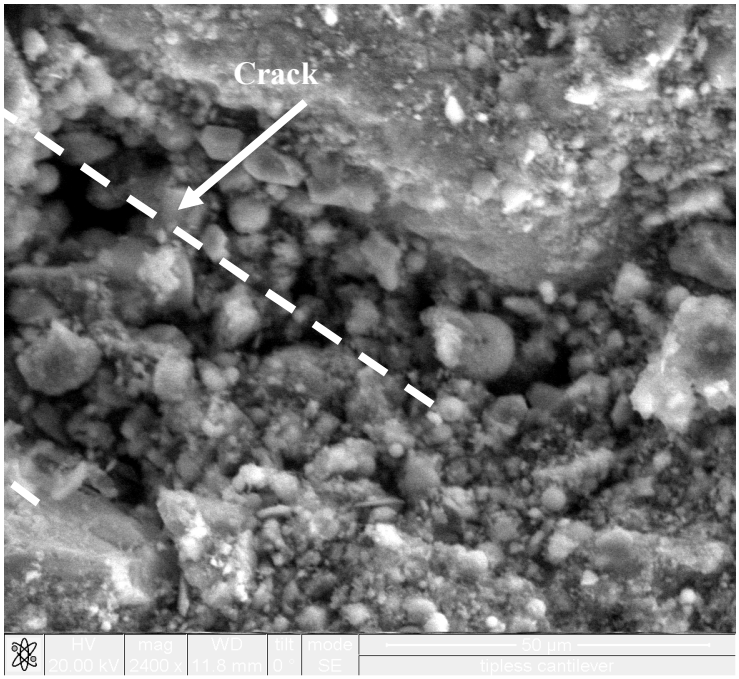

Figure 2.8 - Esem micrograph of rehydration products in a self-healed crack after exposure to salt solution (Şahmaran et al., 2007)

2.4.5 Corrosion Resistance

Reinforcing steel bars embedded in concrete are usually well protected against corrosion by the high alkalinity of pore water because the steel surface is passivated in the presence of oxygen. However, reinforcing steel bars in concrete structures are depassivated when the chloride concentration reaches threshold levels on the rebar surface, or when the pH of the concrete cover drops below critical levels due to carbonation (Tuutti, 1982). Some of the most commonly used protection methods for new constructions against steel reinforcement corrosion include high quality (low water to cement (W/C) ratio and good consolidation) concrete, increased concrete cover thickness, and use of epoxy coated steel reinforcing bars. Generally, low W/C ratio and good consolidation contribute to the reduction in permeability. A higher cover thickness is supposed to provide better physical protection because the concrete acts as a barrier which delays access of chloride ions, carbon dioxide and moisture to the steel reinforcement. However, as a result of restrained shrinkage, thermal deformations, chemical reactions, poor construction practices and mechanical loads, concrete unavoidably cracks and, over time, chlorides, carbon dioxide and moisture can penetrate even high quality concrete or concrete with good cover thickness (ACI 224R, 2001). In addition, a larger cover thickness is known to

lead to a greater crack width. Further, epoxy coatings on the surface of steel reinforcing bars are sometimes damaged during handling, or become brittle and delaminate from the steel reinforcing bars under high chloride concentrations, so that the reliability of epoxy coating for steel protection has been called into question (FHWA, 1992; Saques et al., 1994; Manning, 1996). Consequently, corrosion of reinforcement occurs which could lead to cover spalling and steel diameter reduction, and potentially diminishing of load capacity of the reinforced concrete member. At the root of this steel corrosion problem is the brittle nature of concrete materials. The brittleness of concrete inherently results in cracks that allow corrosives to penetrate the cover, and fail to resist the expansive force once corrosion starts.

With intrinsically tight crack width and high tensile ductility, ECC offers a significant potential to naturally resolving the corrosion related durability problem of reinforced concrete (R/C) structures. Concerned with the large number of microcracks within ECC in comparison to concrete, the rate of corrosion of reinforcing steel within an ECC matrix has been investigated and compared to R/C system (Miyazato and Hiraishi, 2005). Preloaded R/ECC and R/C beams were exposed to a chloride environment to accelerate the corrosion process. To determine the corrosion rate of ECC and concrete, macrocell and microcell corrosion rates were separately determined. The total (macro and micro cell) corrosion rate was measured to be less than 0.0004 mm/year but exceeded 0.008 mm/year in the steel reinforcement in the R/ECC and R/C beams respectively (Figure 2.9).

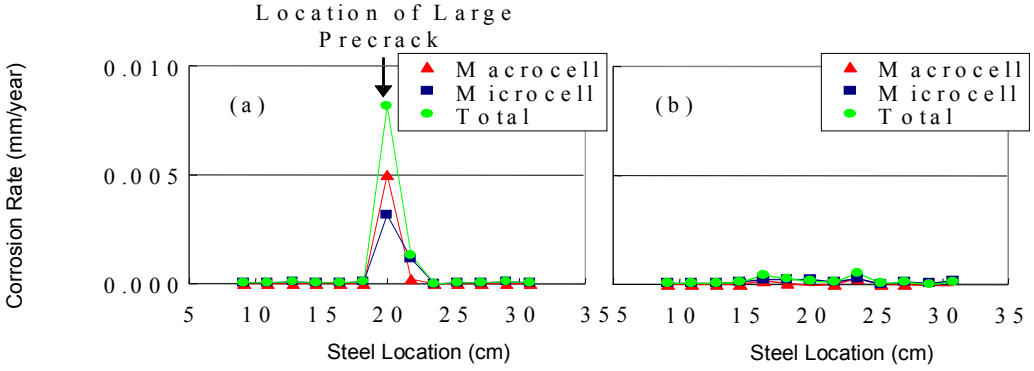

Figure 2.9 Microcell and macrocell corrosion rate measured for (a) R/C, and (b) R/ECC along the reinforcement bar length (Miyazato and Hiraishi, 2005)

In another study, Şahmaran et al. (2008) investigated the cracking behavior and residual flexural load capacities of reinforced ECC (R/ECC) specimens and R/mortar specimens, which have equal compressive strength to the ECC. During accelerated corrosion test at constant applied voltage, corrosion-induced crack width of the mortar specimens were found to increase with time as corrosion activity progressed. Larger crack widths up to 2.00 mm were observed at higher levels of corrosion (Figure 2.10). Moreover, corrosion of reinforced mortar beam specimens resulted in a marked reduction in stiffness and flexural load capacity. After 25 hours accelerated corrosion exposure, the flexural load reduced to about 34 % of the flexural capacity of the control mortar beam. On the other hand, crack widths (~ 0.1 mm) of ECC remained nearly constant with time as corrosion activity progresses, while the number of cracks on the surface of the ECC specimens increased. The results of this study also showed that ECC has significant anti-spalling ability compared with conventional mortar (Figure 2.10). In contrast to mortar specimens, the ECC beam specimens after 50 hours accelerated corrosion exposure retained almost 100% of the flexural capacity of the control specimens. Beyond 50 hours, the flexural capacity decreases, but retained over 45% that of the control specimens even after 300 hours of accelerated corrosion exposure.

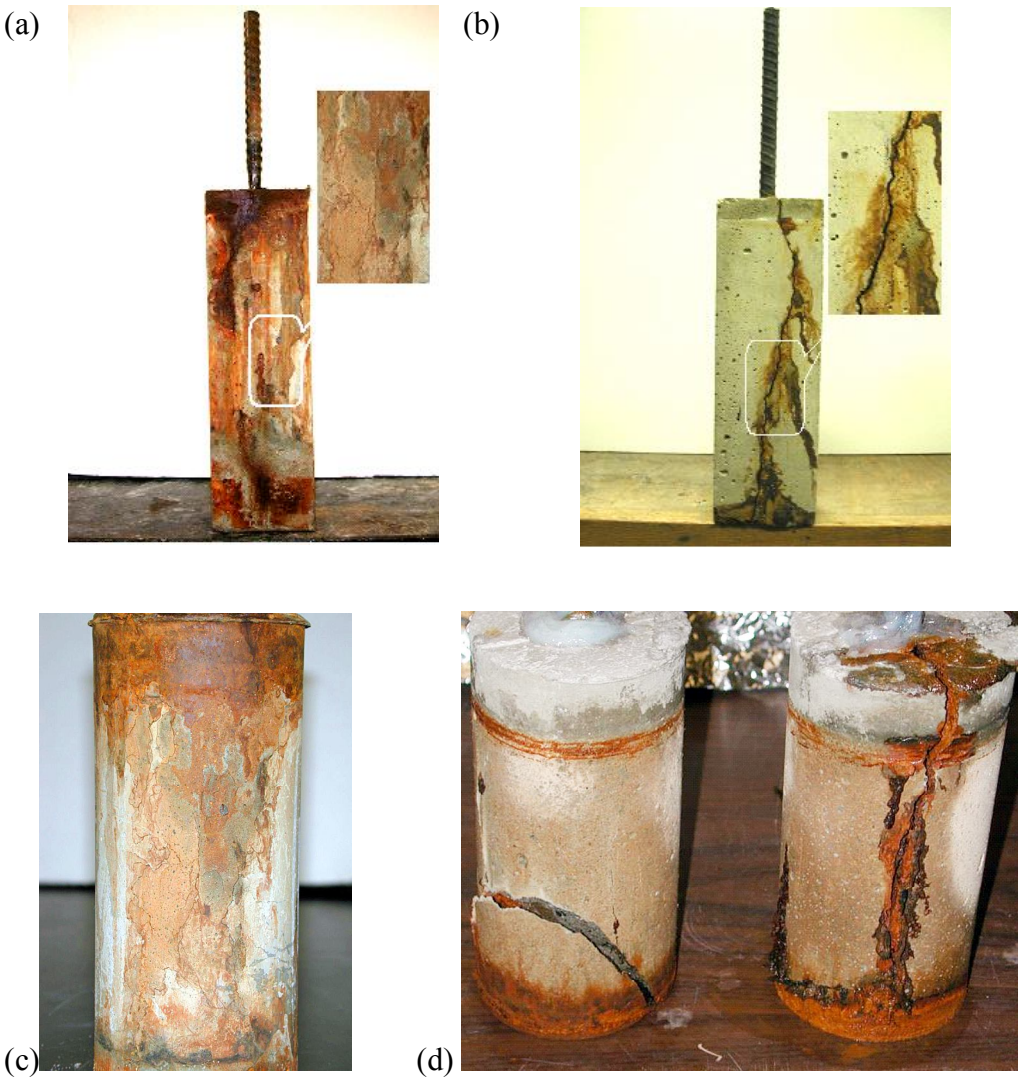

Figure 2.10 ECC and mortar specimens after accelerated corrosion test: (a) ECC prismatic specimen after 300 hours accelerated corrosion, (b) Mortar prismatic specimen after 75 hours accelerated corrosion, (c) ECC cylindrical specimen after 350 hours accelerated corrosion, (d) Mortar cylindrical specimen after 95 hours accelerated corrosion (Şahmaran et al., 2008)

2.4.6 Freeze Thaw and Salt Scaling Resistance

It is well known that the cyclical freeze-thaw cycles and the use of de-icing salts during winter are two of the major causes of rapid degradation in concrete pavements, bridge decks, parking structures, and similar structures. ECC used for this kind of structures must be resistant to cyclical freezing and thawing, and the effects of de-icing agents. It is known that a proper air-void system is generally needed in normal concrete to avoid internal cracking due to freeze-thaw cycles and scaling due to freezing in the presence of deicer salts.

Durability of non-air-entrained ECC specimens was tested by exposure to cycles of freezing thawing testing, in accordance with ASTM C666 (Li et al., 2003). Non-air-entrained concrete specimens were also tested as reference specimens. Non-air-entrained specimens were used as control since no air entrainment was added to the ECC mixtures. After 110 cycles, the concrete specimens had severely deteriorated, requiring removal from the freeze-thaw machine, as mandated by the testing standard. However, all ECC specimens survived the test duration of 300 cycles with no degradation of dynamic modulus. Figure 2.11 shows the typical surface condition of the after 300 freeze-thaw cycles and fog room cured prismatic ECC specimens. This performance results in a durability factor of 10 for concrete compared to 100 for ECC, as computed according to ASTM C666 (1991). In uniaxial tension tests performed on wet cured and freeze-thaw exposed ECC tensile coupons at the same age, no significant drop in strain capacity was experienced after 300 cycles. Both wet cured and freeze thaw specimens exhibited a strain capacity of roughly 3%.

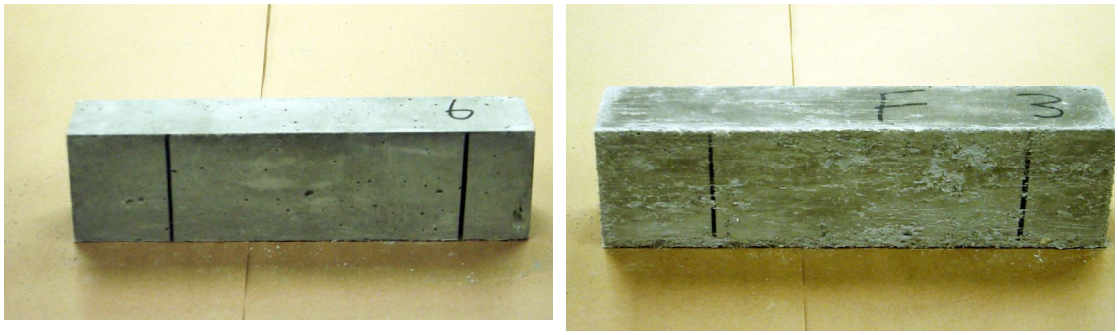

(a) fog room curing (b) after 300 freeze-thaw cycles

Figure 2.11 - ECC specimen surface appearance after (a) normal curing and (b) freeze-thaw cycles

Numerous laboratory test data in accordance with ASTM C 672 (2001) have indicated that air entrained concretes incorporating high volume fly ash often perform unsatisfactorily when exposed to freezing and thawing cycles in the presence of de-icing salts. For the production of ECC, as much as two-thirds of the portland cement is substituted by fly ash. Due to the high volume fly ash content, it is important to test the performance of ECC exposed to freezing and thawing cycles in the presence of de-icing salt. Salt scaling resistance of non-air-entrained sound (uncracked) and mechanically pre-loaded (cracked) ECC specimens was evaluated by Şahmaran and Li in accordance with ASTM C672 (Şahmaran and Li, 2007).

Non-air-entrained mortar specimens with and without fly ash were also tested as reference specimens. After 50 freeze-thaw cycles in the presence of de-icing salt, the surface condition visual rating and total mass of the scaling residue for ECC specimens, even those with high volume fly ash content, remain within acceptable limits of ASTM C672 (Figure 2.12). This level of durability holds true even for ECC specimens pre-loaded to high deformation levels and exhibiting extensive microcracking. In comparison, reference mortar specimens under identical testing conditions deteriorated severely. Moreover, the replacement of fly ash with cement in mortar further exacerbated deterioration due to freezing and thawing cycles in the presence of de-icing salt. In a separate test, both pre-loaded (cracked) and sound ECC coupon specimens were exposed to freeze-thaw cycles in the presence of de-icing salts for 25 and 50 cycles to compare residual tensile strength and ductility of reloaded ECC specimens. The reloaded specimens showed negligible loss of ductility, and retained the multiple micro-cracking behavior and tensile strain capacity of more than 3%. It was also discovered that micro-cracks due to mechanical loading will heal sufficiently under freezing and thawing cycles in the presence of salt solutions, restoring them to nearly the original stiffness. These results confirm that ECC, both sound and micro-cracked, remains durable despite exposure to freezing freeze-thaw cycles in the presence of de-icing salts.

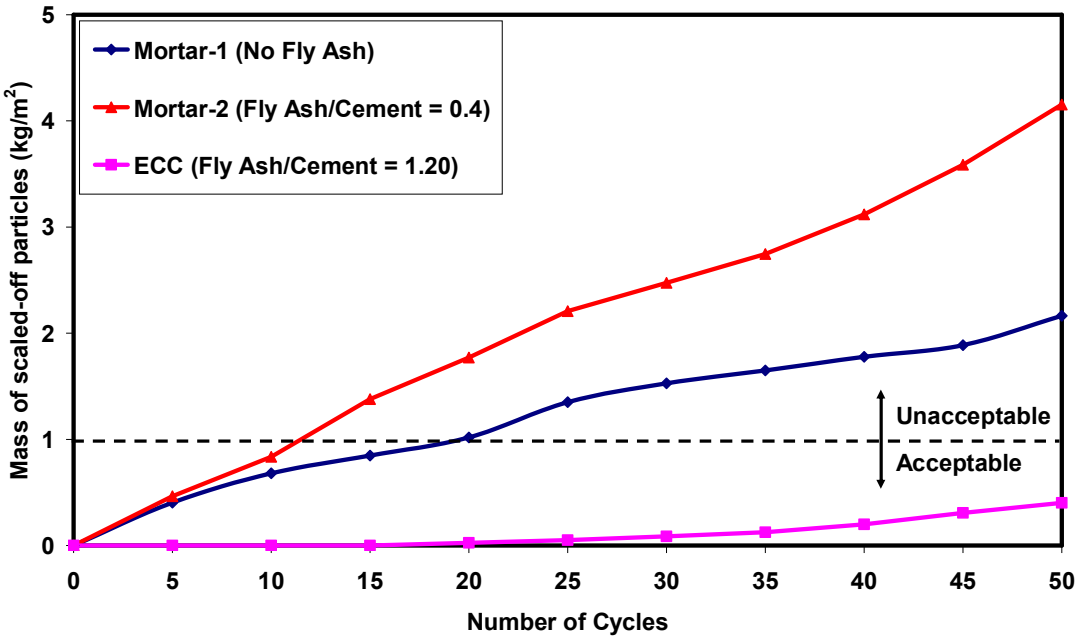

Figure 2.12 - Mass of scaled-off particles versus number of freeze thaw cycles for virgin mortar and virgin ECC prisms in presence of de-icing salts (Şahmaran and Li, 2007)

2.4.7 Durability under Extremely Hot and Humid Environments

In contrast to freeze thaw tests which are designed to simulate temperature changes in winter conditions, hot water immersion tests were conducted to simulate the long term effects of hot and humid environments. To examine the effects of environmental exposure, hot water immersion was performed on individual fibers, single fibers embedded in ECC matrix, and composite ECC material specimens (Li et at., 2004). Specimens for both individual fiber pull-out and composite ECC material were cured for 28 days at room temperature prior to immersion in hot water at 60 ºC for up to 26 weeks. After 26 weeks in hot water immersion, little change was seen in fiber properties such as fiber strength, fiber elastic modulus, and elongation. The tensile strain capacity of the ECC dropped from 4.5% at early age to 2.75% after 26 weeks of hot water immersion. While accelerated hot weather testing does result in lower strain capacity of ECC, the 2.75% strain capacity exhibited after 26 weeks remains over 250 times that of normal concrete.

2.4.8 Durability under Highly Alkaline Environments

Another environment that could affect the microstructure and composite properties of ECC is a high alkaline environment. In addition to high alkaline matrix pore water solution, ECC can come into contact with alkaline media through interaction with a variety of alkaline chemicals, soil (or solutions diffusing through soil) and sea water. Even though no deleterious expansion has been expected due to alkali silica reaction because of the high volume fly ash (HVFA) content, small aggregate particle size and micro-fibers in ECC (Şahmaran and Li, 2008b), durability of HVFA-ECC must be evaluated under high alkaline environments. Alkalis will penetrate through micro-cracks or even the uncracked matrix that could lead to modifications in the material microstructure and hence changes in the composite properties.

Şahmaran and Li (2008b) investigated the durability of ECC under high alkaline environment. The performance of ECC under high alkaline medium was tested according to ASTM C1260-94 (1994). The length change of the ECC bars was measured up to 30 days. Figure 2.13 shows expansive behavior of the ECC. The classification ranges given from the ASTM C 1260-94 (1994) are illustrated

graphically in Figure 2.13 by horizontal gridlines. The results obtained from accelerated mortar bar test indicated that ECC did not show any expansion at the end of 30 days soaking period probably due to non-reactive fine aggregate. However, even if reactive silica sand and alkalis are present in ECC, it cannot be expected to develop deleterious expansion due to alkali silica reaction (ASR) because of the high volume fly ash content, small aggregate particle size and micro-fibers in ECC.

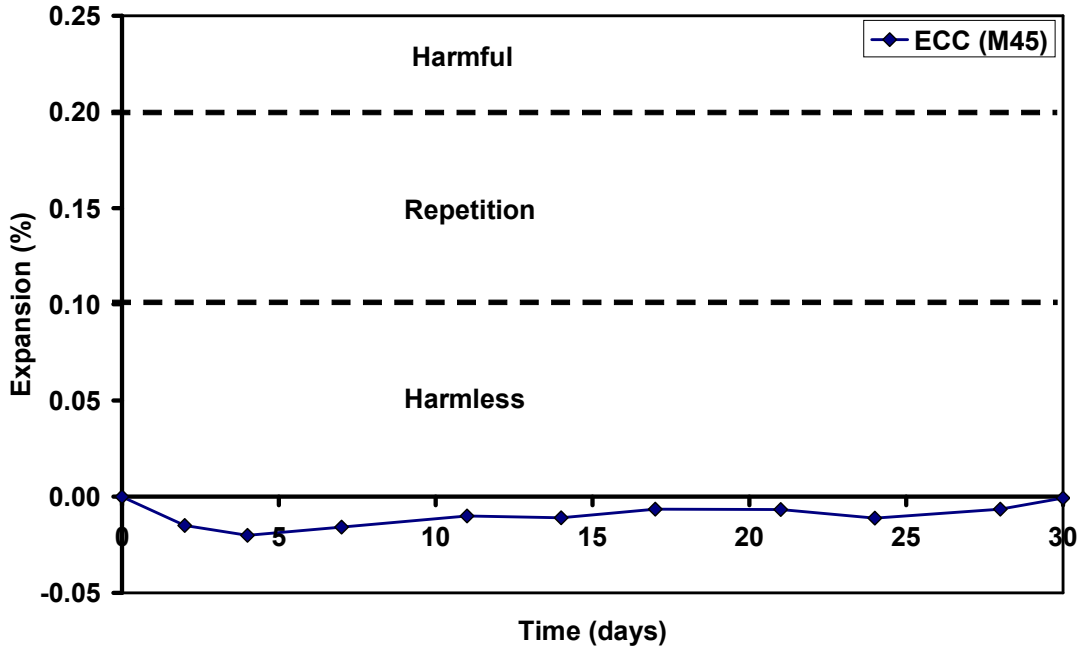

Figure 2.13 Expansion time histories for ECC (ASTM C1260-94) (Şahmaran and Li, 2008-b)

In the same study, Şahmaran and Li (2008b) evaluated the mechanical performance of both virgin and mechanically-loaded ECC under high alkaline environments. ECC coupon specimens were firstly pre-loaded under uniaxial tension to different strain levels, and then exposed to an alkaline environment up to 3 months at 38 ^{o}C and reloaded up to failure. The reloaded specimens showed slight loss of ductility and tensile strength, but retained the multiple micro-cracking behavior and tensile strain capacity of more than 2% (about more than 200 times that of normal concrete and normal fiber reinforced concrete). The test results indicated strong evidence of self-healing of the micro-cracked ECC material, which can still carry considerable tensile stress and strain and restore nearly the original stiffness. This observation is also supported by an environmental scanning electron microscope (ESEM) observation of the fractured surface of ECC across a healed crack. The phenomenon of self-healing

effectively closes the microcracks even after one month sodium hydroxide solution exposure period (Figure 2.14).

Figure 2.14 ESEM micrograph of rehydration products in a self-healed crack after 30-day sodium hydroxide solution exposure period (Şahmaran and Li, 2008-b)

2.5 Applications of ECC

To illustrate the versatility of ECC in real world applications, a number of recent/on-going projects involving the use of ECC are briefly highlighted.

Figure 2.15 shows the repair of the Mitaka Dam in Hiroshima-Prefecture, Japan in April, 2003 (Sakata et al., 2004). This dam is over 60 years old, with a severely damaged concrete surface. Cracks, spalling, and water leakage were concerns that prompted the use of ECC as a water-tight cover layer. This 20 mm layer was applied by spraying the ECC material directly onto approximately 600 m^2 of the upstream dam surface.

Figure 2.15 Spray repair of the Mitaka Dam with ECC for water-proofing (Sakata et al., 2004)

A second large-scale application (Rokugo et al., 2005) in Japan used ECC for repair of a concrete gravity earth-retaining wall (18 m in width and 5 m in height) that has been damaged by (ASR) cracking. The decision to use ECC for the 50-70 mm thick repair was based on the need to prevent reflective cracking from the substrate concrete through the repair layer (Li and Lepech, 2004). Such reflective cracking was anticipated had normal concrete been used for the repair. Since this repair was completed, this project performance has been continuously monitored. Ten and twenty-four months following the repair, microcrack widths in the ECC repair layer remain below 50 μm and 120 μm respectively, while the maximum crack widths in the premixed concrete repair mortar section (used as a control) were 0.2 mm and 0.3 mm, respectively (Kunieda and Rokugo, 2006).

Also in Japan ECC has been used in structural applications as coupling beams (Maruta et al., 2005) within high rise concrete construction. Due to the high energy absorption capacity of steel reinforced ECC material, the application of this material in coupling beams which connect adjacent core walls is very advantageous for high rise buildings in seismic regions. The recent development of precast ECC coupling beam elements by Kajima Corporation in Japan can be easily integrated into current seismic construction practices. Currently two high-rise buildings in Tokyo, Japan have been built integrating ECC coupling beams (Figure 2.16).

Figure 2.16 The Nabeaure Tower in Yokohoma, Japan uses precast ECC coupling beams in building core for seismic resistance

As one of the first field applications of ECC in US, a concrete bridge deck patch was completed in cooperation with the MDOT in 2002. A complete summary of this work has been outlined by Li and Lepech (2004). During this work, one section of a deteriorated bridge deck was repaired with ECC while the remaining portion was repaired with a commercial concrete patching material commonly used by the MDOT (Figure 2.17). This repair scenario allowed for a unique ECC/concrete comparison subjected to identical environmental and traffic loads. The concrete repair material used was a pre-packaged, commercially available repair mortar. At this writing, the repaired bridge deck has experienced more than six complete Michigan winter cycles of freezing and thawing, in addition to live loads. While the ECC patch repair has survived in this combined loading environment with minor microcracking limited to less than 50 μm, the concrete repair portion has developed localized cracks in excess of 3.5 mm wide and required re-repair in 2005.

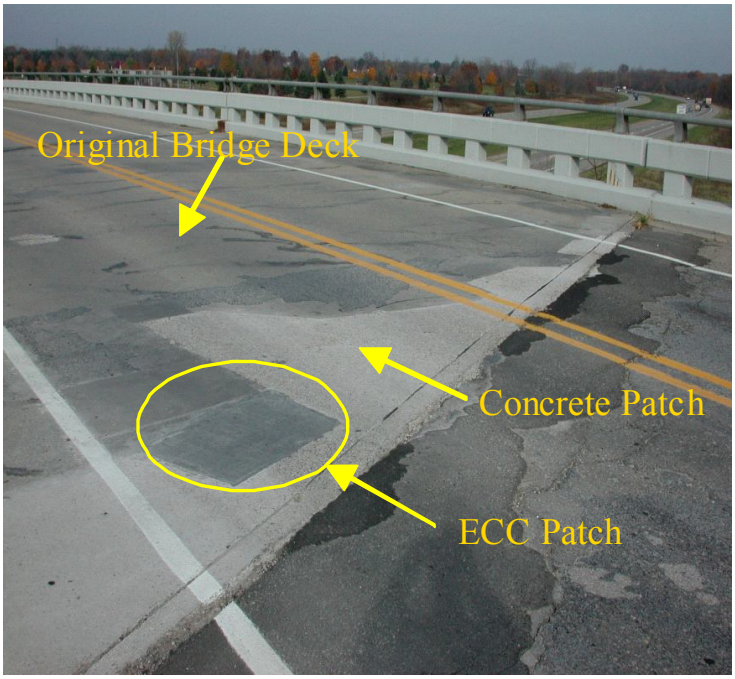

Figure 2.17 ECC patch repair on Michigan bridge deck

In addition to bridge deck patching repairs, the most recent field application of ECC in the US is with a bridge "link slab" completed in cooperation with MDOT in 2005 (Figure 2.18). Within this "link slab", the material ductility of ECC is leveraged to replace problematic expansion joints within simply support multi-span bridges with a ductile ECC slab which links the adjacent simple spans (Li et al., 2005). In this project, about 32 m^3 of ECC were cast in place using standard ready-mix concrete trucks to build the first ECC link slab in US. With a strain capacity exceeding 2%, these composites can be used to replace traditional steel expansion devices and can fully accommodate the thermal deformations of adjacent bridge spans.

(a) during construction (b) after construction

Figure 2.18 ECC link-slab on Grove Street Bridge, Michigan

2.6 Pozzolanic Material

According to ACI 116R-90 (1994), pozzolan is "a siliceous or siliceous and aluminous material, which in itself possesses little or no cementitious value but will, in finely divided form and in the presence of moisture, chemically react with calcium hydroxide at ordinary temperatures to form compounds possessing cementitious properties." Mineral admixtures that are, or both cementitious and pozzolanic can be used as a partial replacement for Portland cement. Some of the most used materials are ground granulated blast furnace slag (slag hereafter), fly ash, condensed silica fume. When properly used as a portion of the cementitious material, these pozzolanic admixtures can improve the properties of the fresh and hardened concrete.

Although several types of supplementary cementitious materials exist, the focus of this review will be on the two types used in this study, namely slag and fly ash. A brief overview of the history, properties, and usage of granulated blast furnace slag and fly ash in concrete is presented in Sections 2.6.1 and 2.6.2.

2.6.1 Slag

Slag has been used as partial replacement for Portland cement in concrete for more than 100 years (Glasser, 1991). As a by-product of the pig iron industry, slag is produced in large quantities in many areas around the world. In the United States, slag is most commonly used as base course for roads and other structures. However, in many other countries, most of the available slag is ground to approximately the same fineness as cement and then utilized as a partial replacement for Portland cement in concrete.

The composition of slag can vary considerably between production facilities. The presence of the major oxides are lypically found to be within the following ranges: magnesium oxide (MgO), 0 to 21 %; aluminum oxide (Al_2O_3), 5 to 33 %; silicon dioxide (SiO_2), 27 to 42 %; and calcium oxide (CaO), 30 to 50 % (Taylor, 1997). Although the composition of slag is important, the method used in its production is perhaps more important as air-cooled slag has very limited, if any, cementing

properties (Moranville-Regourd, 1998). However, if the slag is cooled rapidly from its liquid state at 1350-1550 °C down to about 800 °C, crystallization of the material can be avoided and the resulting product often contains over 95% glass which is a latent hydraulic cement (Taylor, 1997).

For any substantial reaction to occur between slag and water, an activator is required. High alkaline environments have proved to be suitable activators. Fortunately, the pore solution of cement paste is basically composed of alkaline hydroxides and as such, provides for an excellent activator. The use of slag in concrete tends to slow down the rate of hydration at early ages at room temperature. However, elevated temperatures help activate the slag and increase the rate of hydration (Roy, 1992). Therefore, slag can be used in steam-cured concrete. In addition, the damaging effects, such as reduced strength and increased permeability, of high early age temperature on concretes containing slag are less pronounced than when slag is not used (Neville, 1996).

The reaction of a blend of cement and slag results in a higher percentage of calcium-silicate-hydrate (C-S-H) and less calcium hydroxide than plain cement (Neville, 1996). This alteration in the hydration products is attributable to the higher silicon content of the cement and slag blend when compared with plain cement. The change in the microstructure and the slower rate of hydration when slag is used typically yields denser and less permeable concretes.

In addition to lower permeability, concretes made with slag tend to have better resistance to chloride ion penetration than normal concretes. The freeze-thaw resistance of concrete made with slag is believed to be adequate and not adversely affected when compared with concrete made without slag (Neville, 1996). However, concretes made with slag generally suffer higher degree of deicing salt scaling than do reference concretes made without slag (Stark and Ludwig, 1997b). Consequently, ACI Committee 318 (2002) limits the maximum amount of slag to 50 % of the total binder content if the concrete will be exposed to deicing chemicals. The total amount of slag and other supplementary cementitious materials is also limited to a maximum of 50 % of the total binder content.

2.6.2 Fly Ash

Fly ash is the most widely used mineral admixture for concrete. It is a byproduct of burning pulverized coal, in electric power production. During combustion, most of the volatile matter and carbon is burned off leaving the coal's mineral impurities (clay, feldspar, quartz, and shale) behind which then fuse together while in suspension. The fused particles are carried away by the exhaust by electrostatic precipitators or bag filters. During this process the fused material cools and solidifies to form the spherical fly ash particles. Typical particle size is around 20 microns but may range from one micron up to as large as 100 microns. Surface area may range from 200-700 m^2/kg but typically are between 300-500 m^2/kg (Kosmatka and Panarese, 1988).

Fly ash consists primarily of silica, aluminum, iron, and calcium in a silicate glass form. Minor constituents can be found in the form of magnesium, sulfur, sodium, potassium, and carbon. According to American Society for Testing and Materials (ASTM), there are two classes of fly ash (Table 2.2): Class C, which is normally produced from lignite or subbituminous coals and Class F, which is normally produced from bituminous coals (ASTM C 618, 2002). Class C fly ashes differ from Class F fly ashes in that they are self-hardening even without the presence of cement.

Table 2.2 Specifications for fly ash (ASTM C 618, 2002)

Class of Ash	**ASTM Specification**
Class C	$SiO_2 + Al_2O_3 + Fe_2O_3 > 50\%$
Class F	$SiO_2 + Al_2O_3 + Fe_2O_3 > 70\%$

CHAPTER III

EXPERIMENTAL PROGRAM

3.1 Materials

3.1.1 Cement

The cement used in all mixtures was a normal portland cement CEM I 42.5R (C), which correspond to ASTM Type I cement. It had a specific gravity of 3.06 and Blaine fineness of 325 m^2/kg. Chemical composition and physical properties of cement are presented in Table 3.1.

Table 3.1 Chemical properties of Portland cement, fly ash and slag

Chemical composition	**Cement**	**Fly Ash**	**Slag**
CaO (%)	61.43	1.64	34.48
SiO_2 (%)	20.77	56.22	38.40
Al_2O_3 (%)	5.55	25.34	10.96
Fe_2O_3 (%)	3.35	7.65	0.81
MgO (%)	2.49	1.80	7.14
SO_3 (%)	2.49	0.32	1.48
K_2O (%)	0.77	1.88	0.86
Na_2O (%)	0.19	1.13	0.18
Loss of ignition (%)	2.20	2.10	3.00
$SiO_2+Al_2O_3+Fe_2O_3$	29.37	89.21	50.17
Physical properties			
Specific gravity	3.06	2.31	2.79
Blaine fineness (m^2/kg)	325	290	425

The particle size distributions of cement, obtained by a laser scattering technique, is given in Figure 3.1.

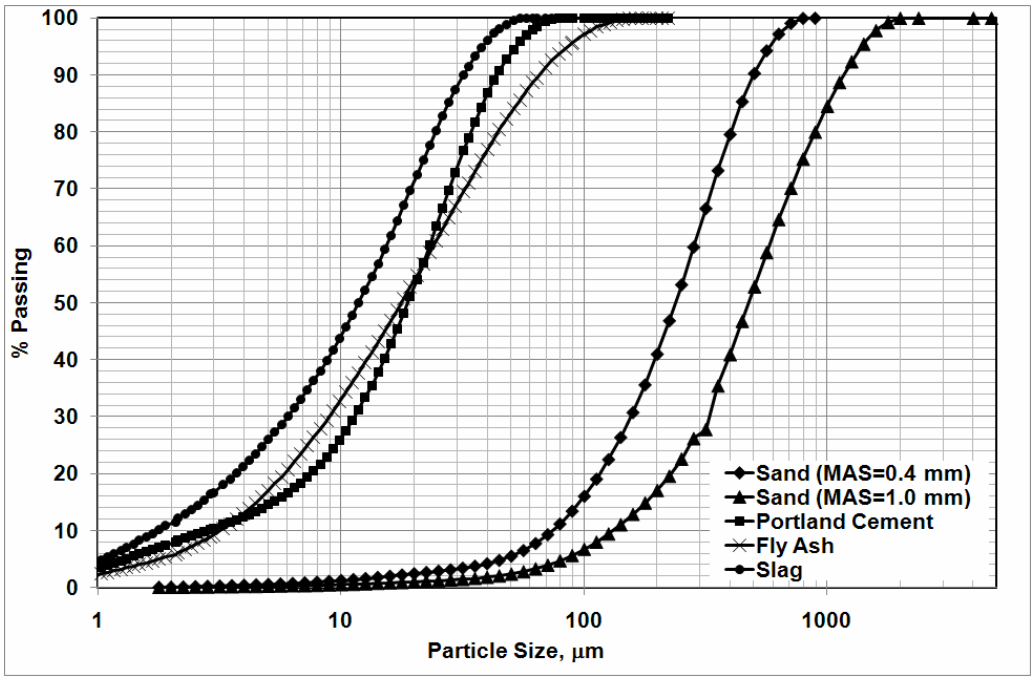

Figure 3.1 Particle size distributions of fly ash, slag and aggregates

3.1.2 Mineral Admixtures

3.1.2.1 FlyAsh

Class-F fly ash (FA) conforming to ASTM C 618 (2003) requirements with a lime content of 1.64% obtained from Sugözü Thermal Power Plant was used. The chemical properties of FA are given in Table 3.1. The specific gravity and Blaine fineness of FA are 2.31 and 290 m^2/kg, respectively. The particle size distribution of FA is provided in Figure 3.1. Figures 3.2 illustrates the particle morphology of FA. The scanning electron microscope (SEM) image showed that the particles of FA had significantly smooth spherical particles in comparison to slag.

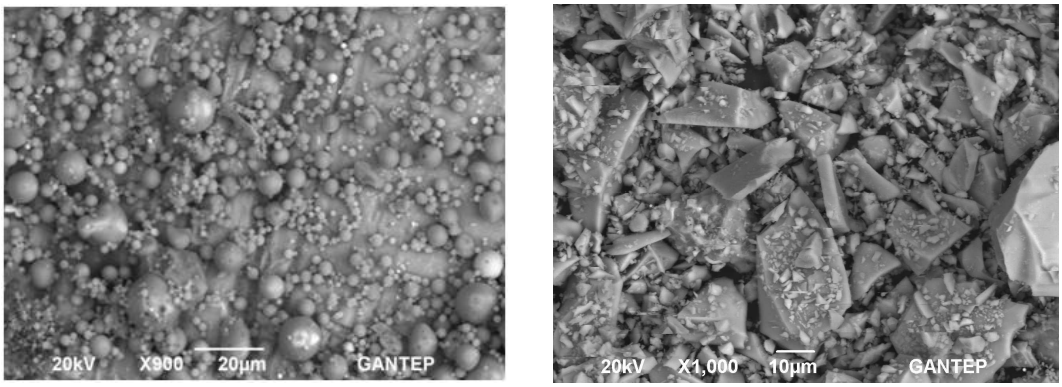

Fly Ash Slag

Figure 3.2 Particle morphology of fly ash and slag determined by SEM

3.1.2.2 Slag

Slag (S) was supplied from Iskenderun Iron–Steel Factory in Turkey. Its chemical oxide composition is given in Table 3.1. The specific gravity of slag was 2.79 g/cm^3 The slag was ground granulated in Iskenderun Cement Factory to have a Blaine specific surface area about 425 m^2/kg. According to ASTM C 989 (2009) hydraulic activity index, the slag used was classified as a category 80 slag. Particle size distribution of slag obtained by using the laser diffraction is shown in the Figure 3.1. To identify morphological characteristics of slag, it was analyzed with SEM and the resulting photograph is presented in Figure 3.2.

3.1.3 Aggregate

According to micromechanic-based design of ECC, exhibiting ductile and showing a large crack number, but small in width, of cementitious composites a low toughness of the matrix is required. However, with the increasing of maximum grain size of aggregate, increase in toughness of the matrix is appeared and as a result, to obtain suitable ECC, aggregate grain size is limited (Li et al.,1995). Therefore, so far, ECC has been produced successfully with an average grain size of about 110 μm (Li et al.,1995). Using high volumes of industrial by-product in the production of ECC decreases matrix toughness and provides freedom of changing aggregate size. It is very important to produce ECC from normal size local sources of aggregate in terms of widespread application for both literature and our country. For this purpose, in the production of ECC, fine quartz with two maximum aggregate sizes (MAS) of 400 μm and 1000 μm was obtained from local sources in our country's resources. Water absorption capacity and specific weight of quartz aggregate used is 0.3% and 2.60, respectively. The grain size distribution curves for these aggregates are presented in Figure 3.1.

3.1.4 Chemical Admixtures

To improve the workability of ECC mixtures, Glenium 51, high range water reducing admixture (HRWR – polycarboxylate ether as an active ingredient with 1.1 specific gravity and 40% solid content) produced by BASF Construction Chemicals was used.

3.1.5 Polyvinyl Alcohol (PVA) Fiber

Although various fiber types have been used in the production of ECC, PVA fiber was used in this study (Figure 3.3). The use of PVA fiber was decided based on and PVA-ECC represents the most practical ECC used in the field (Li et al., 2001; Kunieda and Rokugo, 2006) at the present. PVA fibers have attracted most attention due to the outstanding composite performance and economics consideration. The dimensions of the PVA fiber are 8 mm in length and 39 μm in diameter. The nominal tensile strength of the fiber is 1620 MPa and the density of the fiber is 1300 kg/m^3. The mechanical and geometric properties of PVA fibers are summarized in Table 3.2. The PVA fiber is surface-coated by hydrophobic oil (1.2% by weight) in order to reduce the fiber/matrix interfacial bond strength. To account for material inhomogeneity, a fiber content of 2% by volume in excess of the calculated critical fiber content has been typically used in the mix design. These decisions were made through ECC micromechanics material design theory and had been experimentally demonstrated to produce good ECC properties in previous investigations (Li et al., 2001; Kong et al., 2003a).

Figure 3.3 PVA Fiber used in the production of ECC

Table 3.2 Mechanic and Geometric Properties of PVA Fibers

Fiber Type	Nominal Strength (MPa)	Apparent Strength (MPa)	Diameter (μm)	Length (mm)	Young Modulus (GPa)	Strain (%)	Specific Weight kg/ m^3
PVA	1620	1092	39	8	42.8	6.0	1300

3.2 ECC Mixing and Specimen Preparation

The experimental program was based on a 2 (MAS) × 3 (aggregate/binder ratio) × 2 (mineral admixture types) × 2 (mineral admixture replacement rate). In total twenty-four mixtures with two different aggregate sizes (0.4 and 1.0 mm MAS), three aggregate contents (0.36, 0.45 and 0.55 aggregate-binder ratios), two mineral admixture types (FA and slag), and two mineral admixture replacement rate (1.2 and 2.2 FA or S – C ratio) were considered in this study. Details of this factorial design and designation of mixtures are presented in Table 3.3. In all mixtures the water-binder ratio (W/B) were the same. To obtain approximately similar workability and uniform disperse of fibers, the HRWR content was varied from mix to mix. As seen from Table 3.3, the ECC mixture with the lowest slag content (S/C ratio of 1.2) had the highest HRWR demand, but as part of the cement was replaced by FA or slag replacement rate was increased, the HRWR content of mixtures decreased. The smooth surface characteristics and spherical shape of the FA improved the workability characteristics of ECC mixtures, so that similar workability properties at constant W/B ratio were achieved by using a lower HRWR content at higher FA replacement level (Figure 3.2).

As shown in Table 3.3, the ECC mixtures are labeled such that the ingredients are identifiable from their Mix IDs. The first letter in the mixture designations indicates the mineral admixture type (FA = fly ash, S = slag). The numbers after the letter indicate the mineral admixture (FA or S) – cement ratio, aggregate/binder (A/B) ratio and maximum aggregate size, respectively. The mix proportion of a standard ECC mixture FA1.2_0.36_400 (M45) (Table 3.3) Wang and Li (2007) is used as a reference in the ECC mix design.

Table 3.3. ECC mixture proportions containing fly ash and slag by weight

Mix ID.	Cement	W/B	Aggregate/Binder		FA/C	S/C	HRWR
			0-400 μm	0-1000 μm			kg/m^3
FA1.2_0.36_400 (M45)	1	0.27	0.36	-	1.2	-	5.1
FA1.2_0.45_400	1	0.27	0.45	-	1.2	-	5.1
FA1.2_0.55_400	1	0.27	0.55	-	1.2	-	5.0
FA1.2_0.36_1000	1	0.27	-	0.36	1.2	-	4.9
FA1.2_0.45_1000	1	0.27	-	0.45	1.2	-	5.0
FA1.2_0.55_1000	1	0.27	-	0.55	1.2	-	5.0
FA2.2_0.36_400	1	0.27	0.36	-	2.2	-	3.0
FA2.2_0.45_400	1	0.27	0.45	-	2.2	-	3.0
FA2.2_0.55_400	1	0.27	0.55	-	2.2	-	3.0
FA2.2_0.36_1000	1	0.27	-	0.36	2.2	-	3.0
FA2.2_0.45_1000	1	0.27	-	0.45	2.2	-	3.0
FA2.2_0.55_1000	1	0.27	-	0.55	2.2	-	3.0
S1.2_0.36_400	1	0.27	0.36	-	-	1.2	5.8
S1.2_0.45_400	1	0.27	0.45	-	-	1.2	5.9
S1.2_0.55_400	1	0.27	0.55	-	-	1.2	6.0
S1.2_0.36_1000	1	0.27	-	0.36	-	1.2	4.9
S1.2_0.45_1000	1	0.27	-	0.45	-	1.2	5.0
S1.2_0.55_1000	1	0.27	-	0.55	-	1.2	5.0
S2.2_0.36_400	1	0.27	0.36	-	-	2.2	4.7
S2.2_0.45_400	1	0.27	0.45	-	-	2.2	4.1
S2.2_0.55_400	1	0.27	0.55	-	-	2.2	4.3
S2.2_0.36_1000	1	0.27	-	0.36	-	2.2	3.5
S2.2_0.45_1000	1	0.27	-	0.45	-	2.2	3.6
S2.2_0.55_1000	1	0.27	-	0.55	-	2.2	4.0

HRWR: High range water reducing admixture, C: Cement, FA: Fly Ash, S: Slag

In this study, a Hobart type mixer (Figure 3.4) with 20-liter capacity was used in preparing all ECC mixtures. Solid ingredients, including cement, mineral admixture (FA or S), and aggregate, were first mixed at 100 rpm for a minute. Water and HRWR admixture were then added into the dry mixture and mixed at 150 rpm for one minute and then at 300 rpm for another two minutes to produce a consistent and uniform ECC matrix (without PVA fiber). PVA fiber was added in last and mixed at 150 rpm for an additional three minutes.

Mixing of solid ingredients

Water addition

HRWR addition

Fiber addition

Figure 3.4 Production of ECC by using Hobart Type mixer

At least six specimens of each ECC mixture were tested under each type of loading condition for each testing age (7, 28, 90 and 180 days). 50-mm cubic specimens were prepared for the compressive strength test, 360×50×75 mm prism specimens were prepared for the four-point bending and fracture toughness tests. Also, for each mixture three 285×25×25 mm bar specimens and two ring specimens were cast to determine drying shrinkage and restrained shrinkage cracking potential, respectively. All specimens were demolded after 24 hours, and moisture cured in plastic bags at 95±5 % RH, 23±2 ^{o}C for 7 days. The specimens were then air cured at 50±5 % RH, 23±2 ^{o}C until the day of testing (Figure 3.5).

Figure 3.5 Curing of ECC specimens after production of them

3.3 Test Procedure

3.3.1 Compressive Strength

Twenty four cubic samples (6 specimens for each of age) of 50 mm were cast from each ECC mixture. The compression test was carried out on the cubic specimens by using a 3000 kN capacity testing machine in accordance with ASTM C39 (2003) (Figure 3.6). ECC cubic samples were tested for compressive strength measurement at the age of 7, 28, 90 and 180 days.

Figure 3.6 Compression testing machine and cubic samples

3.3.2 Fracture Toughness

To measure the fracture toughness of ECC matrix (ECC without PVA fiber), eighteen prismatic samples (6 specimens for each age of testing) having dimensions of 360x75x50 mm were prepared. There is no method in the standards in order to measure stress intensity factor of cementing materials. Therefore, in this study to measure stress intensity factor, ASTM E399 (2003) "Linear-Elastic Plane-Strain Fracture Toughness K_{IC} of Metallic Materials," Standard test method was used. This standard test method for cement matrix has been previously implemented in a detailed manner and applicability of it to such systems has been verified. Set-up for measuring fracture toughness is presented in Figure 3.7. According to this test method 6 samples of 360x75x50 mm size, in center of which about 30 mm deep notch was opened, were prepared for each age of 28, 90 and 180 day. Then these samples were tested at a three-point bending test at a rate of 0.002 mm / sec. After this test, exact depth of notch of samples was measured and then the toughness of the matrix was calculated.

Fracture toughness of the specimens was calculated in accordance with following Equation (3.1):

$$K_Q = \frac{P_Q S}{B W^{\frac{3}{2}}} \cdot f\left(\frac{a}{W}\right) \tag{3.1}$$

P_Q: Applied load, S: Span width, B: Height of the specimen, W: Depth of the specimen, and $f\left(\frac{a}{W}\right)$: geometric calibration factor (varying between 1.91 and 2.18 with respect to determined exact depth of the specimens)

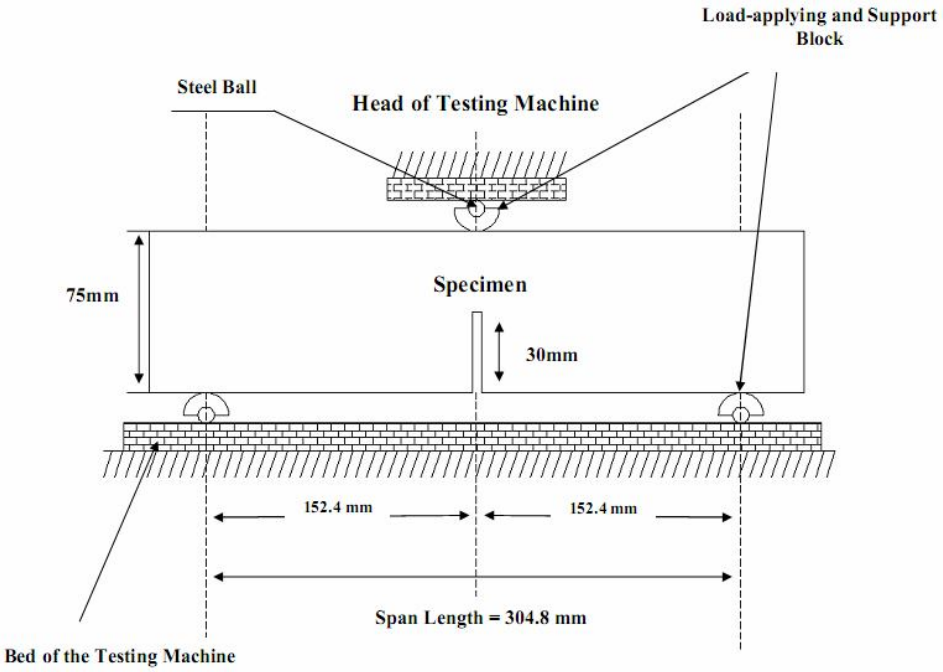

Figure 3.7 Test set-up of determining fracture toughness

3.3.3 Flexural Performance

To measure the flexural performance of ECC mixture, twenty four prismatic samples (6 specimens for each age of testing) having dimensions of 360x75x50 mm were cast from each produced ECC mixture. ECC prisms were first cleaned, and then flexural strength under four-point test was performed by using universal testing system (Figure 3.8).

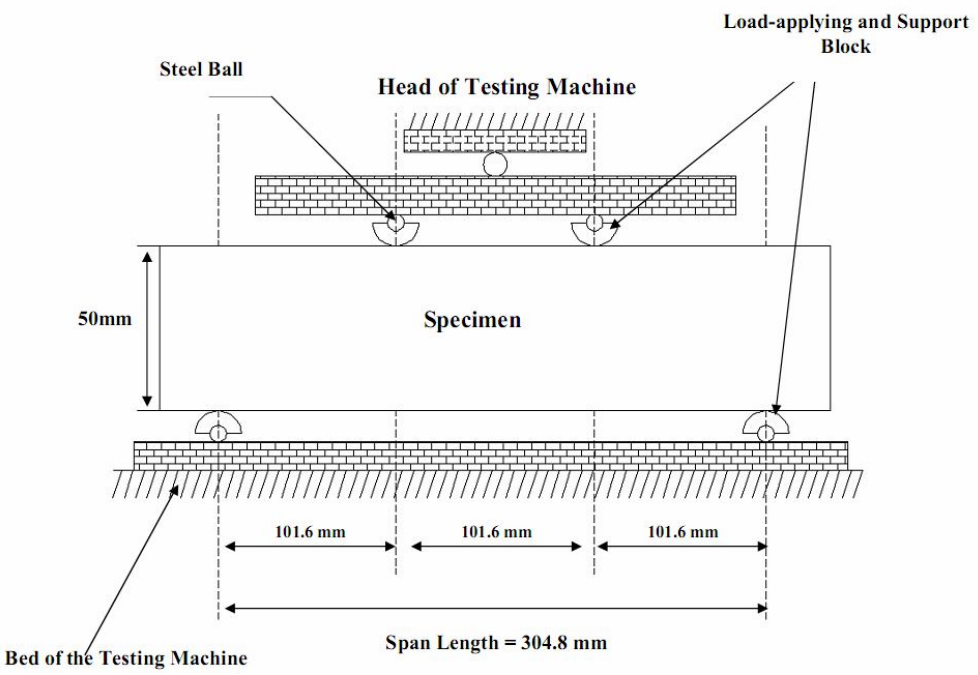

Figure 3.8 Four-point bending test setup

Four point bending test was performed on a closed-loop controlled material test system at a loading rate of 0.005 mm/s. The capacity of the loading frame was 100 kN (Figure 3.9). A four point bending loading fixture was developed to eliminate extraneous deformations such as support settlements and specimen rotations. The span length of flexural loading was 304 mm with a 101 mm center span length. During the flexural tests, the load and mid-span deflection were recorded on a computerized data recording system. Linear variable displacement transducer (LVDT) was fixed on the test set-up to measure the flexural deflection of the specimen. After bending tests, crack widths on the surface of the specimens were also measured by using a macroscope (Figure 3.10). To evaluate composite performances, microstructural analysis in terms of scanning electron microscopy (SEM) and mercury intrusion porosimetry (MIP) were also performed on selected mixture. The results obtained from the mechanical tests and microstructural analysis at the aggregate-matrix and fiber-matrix interfaces lead to a better understanding of behavior, and may be used in the improvement of mechanical performance and ductility of ECC.

Figure 3.9. Four-point flexural strength test

Figure 3.10. Control of crack widths of specimens tested by four-point test

3.3.4 Drying Shrinkage

The drying shrinkage of bar specimens was measured up to 180 days after an initial curing of one day in the mould and 27 days in lime saturated water by using three 285×25×25 mm prismatic specimens in accordance with ASTM C157 (2004) for all ECC mixtures (Figure 3.11). Gauge studs were inserted in the bar moulds coaxial with the bar before the ECC mixtures was poured in to the moulds. The drying shrinkage specimens were stored in laboratory at 23±2 ^{o}C, and 50±5% relative humidity.

Figure 3.11 Drying shrinkage device and samples

3.3.5 Restrained Ring Shrinkage

Although there is no standard test to assess cracking due to restrained shrinkage, several restrained shrinkage test methods have been proposed to measure the shrinkage cracking behavior of concrete (Malhotra, 1970; Kraai, 1985; Carlson and Reading, 1988). In this work, ring tests were used to assess the potential for restrained shrinkage cracking. Restraining ring was made of ECC ring (140 mm in height) cast around the outer perimeter of a steel ring with 280 mm and 305 mm inner and outer diameters, respectively. A 25.4 mm thick layer of ECC was cast around a 12.5 mm thick steel annulus. For each type of ECC mixture, two rings were cast and cured in the molds for 24 hours. The exterior mold was removed 24 hour after casting and the top surface of the ring was sealed using a silicone-based sealant. The rings were then placed in an environmental chamber at 50 ± 5% relative humidity (RH) and 23±2 ^{o}C. Therefore, drying was allowed only from the outer circumferential surface of the ring-type concrete for restrained shrinkage specimens. It should be noted that the curing conditions for the ring tests are different from the free drying shrinkage test. The purpose of the early demolding and short curing time in the ring tests is to simulate the early re-opening conditions in field application. The restrained shrinkage was used to record the onset time of a new crack and the time development of the width at the crack mouth. The cracking pattern, crack number and crack width were measured as a function of age with a hand held microscope. Measurements were taken every 24 hour for 28 days at three different

locations along each crack and the average value was plotted. A schematic restrained ring test setup is shown in Figure 3.12.

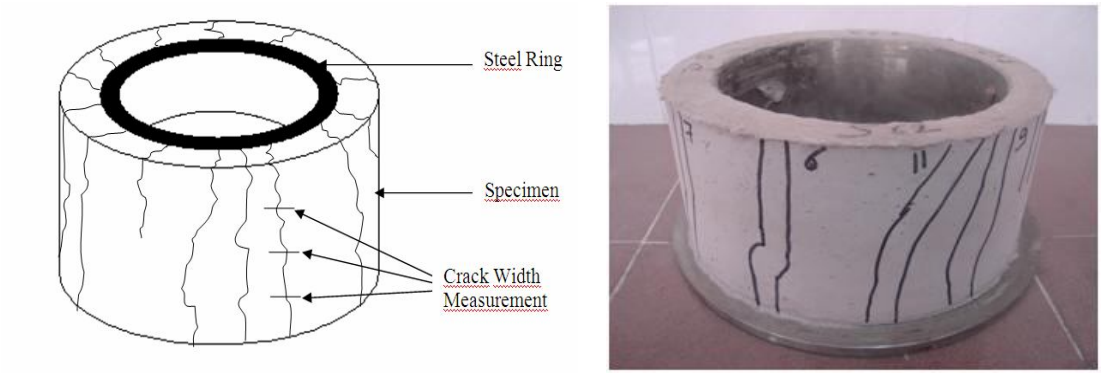

Figure 3.12 Restrained shrinkage test setup

CHAPTER IV

RESULTS AND DISCUSSIONS

4.1 Compressive Strength

The compressive strength test results of the ECC mixtures incorporating different MAS and amount, and FA and S contents are summarized in Table 4.1.

Table 4.1. Compressive strength test results of ECC mixtures

Mix ID.	Compressive Strength (MPa)			
	7 days	28 days	90 days	180 days
FA1.2_0.36_400 (M45)	40.1	69.3	75.8	78.6
FA1.2_0.45_400	40.9	69.8	72.5	76.2
FA1.2_0.55_400	37.4	62.6	67.6	73.8
FA1.2_0.36_1000	37.4	60.8	65.5	71.4
FA1.2_0.45_1000	40.0	63.5	66.8	71.9
FA1.2_0.55_1000	41.6	69.4	72.7	77.3
FA2.2_0.36_400	30.2	46.1	54.7	59.1
FA2.2_0.45_400	29.0	45.8	56.8	62.3
FA2.2_0.55_400	30.3	47.9	58.7	63.4
FA2.2_0.36_1000	27.9	48.7	57.7	63.1
FA2.2_0.45_1000	29.3	50.5	56.5	61.8
FA2.2_0.55_1000	28.6	47.5	54.2	60.3
S1.2_0.36_400	59.9	88.5	91.2	92.1
S1.2_0.45_400	58.0	90.0	93.2	95.2
S1.2_0.55_400	56.9	86.5	90.7	92.6
S1.2_0.36_1000	60.0	89.6	92.2	95.1
S1.2_0.45_1000	58.1	91.4	94.2	95.8
S1.2_0.55_1000	58.5	87.9	91.1	94.3
S2.2_0.36_400	51.8	76.3	80.3	83.7
S2.2_0.45_400	50.6	78.5	88.7	88.9
S2.2_0.55_400	52.8	81.5	86.6	88.6
S2.2_0.36_1000	52.9	79.4	84.2	87.1
S2.2_0.45_1000	50.4	78.0	88.1	89.6
S2.2_0.55_1000	52.6	79.2	82.3	85.3

Compressive strength tests were performed at 7, 28, 90 and 180 days of age. Six cylinder specimens were tested at each age for each mixture. As seen from Table 4.1 and as expected, at same replacement level, especially at early ages, the slag produced significantly greater strengths than the FA. The greatest difference was observed at 7 days for the replacement level of 2.2, where the S-ECC specimens achieved more than 70% higher compressive strengths than those containing FA. All the mixtures, however, showed compressive strengths higher than 45 MPa at 28 days of age. This value could significantly exceed that of normal concrete strength (30 MPa), and fulfill engineering requirements in most projects.

The strength development characteristics of FA-ECC and S-ECC containing different amount and sizes of aggregate with time were normalized as the ratio of average compressive strength data of ECC mixtures with same mineral admixture type and replacement level at various curing ages to those at 7 days and the normalized values were presented in Figure 4.1. Therefore, at each age, % compressive strength gain (relative to compressive strength at 7 days) versus age data could be plotted. Figure 4.1 indicated a continued increase in strength even after 28 days for ECC mixtures with FA while the compressive strength appeared to approach an asymptotic value after 28 days of age in the ECC mixtures with slag. The FA-ECC mixtures had significant strength gain from 28 days to 180 days, while the S-ECC had already achieved more than 90% of their 180-day strength at 28 days. This finding was partially a result of the advances in hydration and pozzolanic reactions of the slag compared to that of ECC containing FA. However, from the strength gain observed in ECC mixtures it could be stated that significant improvements in the compressive strength and the rate of strength gain were obtained by increasing the volume of FA.

As seen from Table 4.1, an increase in the MAS and aggregate amount had no consistent effect in the compressive strength of ECC mixtures, and at same mineral admixture type and amount mixtures yielded very similar compressive strength test results. This behavior was consistent for all mineral admixture replacement level. This finding was likely the result of a limited supply of mix water available for hydration reactions or the hydration by-product required for pozzolanic reactions. If, for example, one examines mix S2.2_0.55_1000, shown in Table 4.1, which have the same W/B ratio and slag replacement rate as S2.2_0.36_1000 and less binder (S + C)

content because of higher aggregate/binder ratio, one could deduce that the compressive strength of ECC mixtures with high cementing material was mostly influenced by the limited space available for hydration processes. This consequently would result in a high percentage of unhydrated particles in all ECC mixtures with a high binder content of more than 1100 kg/m^3. It was also known that conventional concrete strength was affected when the aggregate size becomes large or small. Smaller aggregate size, and consequently, higher surface area for a given aggregate content, resulted in lower bond stress at a given load level (Cetin and Carrasquillo, 1998). In addition, everything else being the same, the larger the aggregate size the higher the local water-cement ratio in the interfacial transition zone and, consequently, the weaker the concrete (Mehta and Monteiro, 2006). Therefore, unlike conventional concrete, aggregate amount (0.36, 0.45 and 0.55 aggregate-binder ratios) and aggregate size (0.4 and 1.0 mm maximum particle sizes) did not influence the compressive properties in the case ECC within the limited aggregate amount and size employed in the present experiments.

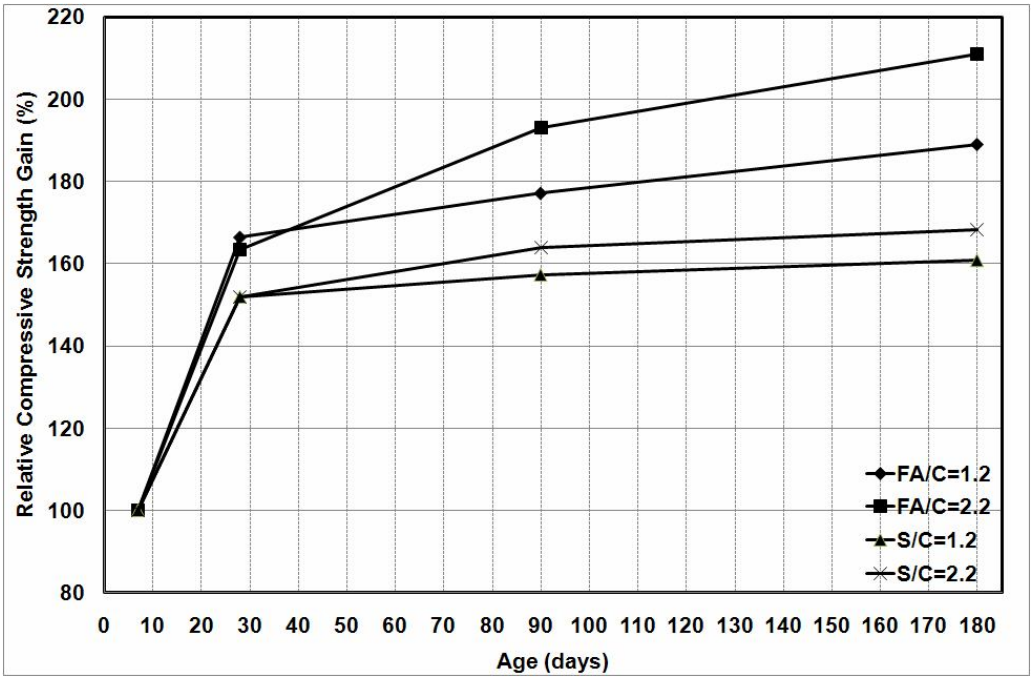

Figure 4.1. Compressive strength increase of ECC mixtures with the age

4.2 Fracture Toughness

Fracture toughness tests were conducted on ECC matrix specimens (ECC w/o fiber) at 28, 90 and 180 days after production of them. Tests were performed in accordance with the ASTM E 399 (2003). The fracture toughness test results of the ECC mixtures incorporating different aggregate sizes and amount, and FA and slag contents were summarized in Table 4.2. Figure 4.2 illustrated the effects of FA, slag, MAS and aggregate amount on the fracture toughness of ECC matrixes as a function of the age of the matrix. The figure showed that the fracture toughness of the ECC matrixes containing slag was consistently more than the fracture toughness of the ECC matrixes containing FA. This was mainly due to the enhanced matrix strength even at early ages caused by the presence of slag particles. Slag particles were most commonly activated by the hydration product of Portland cement, where calcium hydroxide formed during hydration was the principal activator. Slag hydration products lead to decreased porosity in the matrix, resulting in enhanced matrix strength and toughness. Higher matrix toughness could be detrimental to achieving the desired mechanical properties, and reducing the margin to develop multiple-cracking in terms of toughness ratio (Li et al., 1995). Therefore, in order to satisfy the limits on the matrix toughness in slag-ECC, aggregate particle size had to be reduced or amount of slag replacement had to be increased, which consequently lead to a relatively low matrix fracture toughness values. Test results also indicated that the use of FA particles should be helpful for achieving strain-hardening behavior, as a lower fracture toughness value provided better opportunities for multiple cracking in the composite. It also demonstrated that fracture toughness was nearly constant as a function of age (in this case, for ages of 90 to 180 days).

Table 4.2 Fracture toughness test results of ECC matrix mixtures

Mix ID.	Fracture Toughness ($MPa \times m^{1/2}$)		
	28 days	**90 days**	**180 days**
FA1.2_0.36_400 (M45)	0.536	0.662	0.683
FA1.2_0.45_400	0.580	0.712	0.741
FA1.2_0.55_400	0.627	0.788	0.799
FA1.2_0.36_1000	0.624	0.700	0.723
FA1.2_0.45_1000	0.649	0.721	0.738
FA1.2_0.55_1000	0.707	0.772	0.807
FA2.2_0.36_400	0.356	0.534	0.596
FA2.2_0.45_400	0.424	0.551	0.619
FA2.2_0.55_400	0.522	0.647	0.667
FA2.2_0.36_1000	0.452	0.575	0.611
FA2.2_0.45_1000	0.494	0.600	0.638
FA2.2_0.55_1000	0.546	0.642	0.684
S1.2_0.36_400	0.795	0.801	0.809
S1.2_0.45_400	0.827	0.839	0.847
S1.2_0.55_400	0.840	0.898	0.904
S1.2_0.36_1000	0.778	0.817	0.848
S1.2_0.45_1000	0.879	0.899	0.917
S1.2_0.55_1000	0.873	0.944	0.961
S2.2_0.36_400	0.712	0.728	0.748
S2.2_0.45_400	0.715	0.756	0.766
S2.2_0.55_400	0.747	0.795	0.811
S2.2_0.36_1000	0.726	0.799	0.809
S2.2_0.45_1000	0.753	0.807	0.821
S2.2_0.55_1000	0.857	0.891	0.914

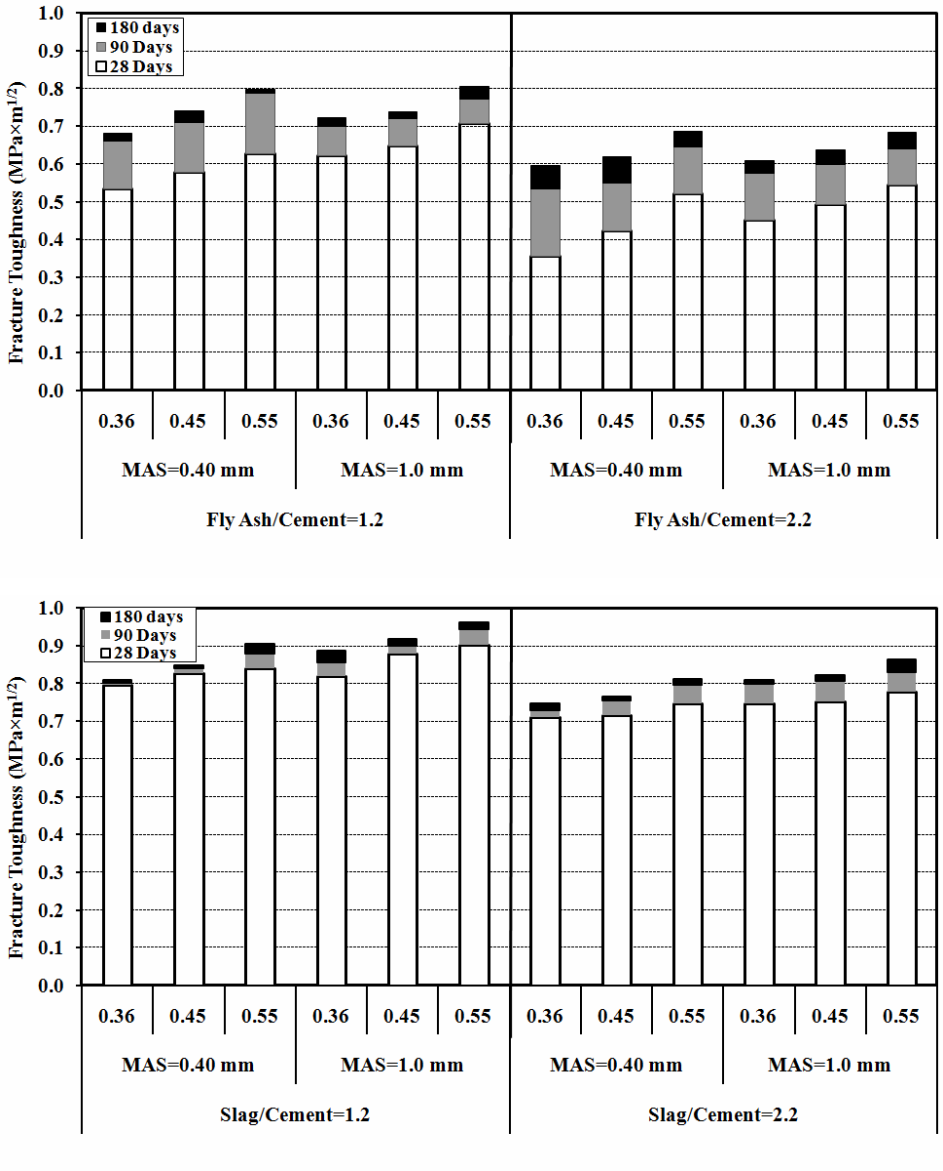

Figure 4.2 Matrix fracture toughness – K_m as a function of the matrix age

The fracture energy of ECC matrixes with the same replacement rate of mineral admixtures increased significantly as the aggregate-binder ratio changed from 0.36 to 0.55, and aggregate size changed from 0.4 mm to 1.0 mm. Especially at low strength level (for example, ECC mixtures with FA/C ratio of 2.2), matrix fracture toughness values significantly increased with the increase of aggregate amounts and sizes. It is well known that when concrete is loaded, cracks prefer to propagate along the weaker interfacial zone or big larger pores in the matrix (Davis and Alexander, 1989; Davis and Alexander, 1992; De Larrard and Belloc, 1997). As the crack meets an aggregate particle, it is forced either to propagate through the tougher aggregate or deflect and travel around the aggregate-mortar interface. For low strength concrete,

the interfacial zone is weaker than the aggregate. Cracks prefer to propagate along the interfacial zone, while the aggregates debond, and then deflect and bridge cracks. Therefore, when aggregate volume increases, more aggregates debond and deflect cracks, resulting in more tortuous cracking path and more energy needed for cracking, and then higher values of fracture toughness. The larger maximum size of aggregate, the more tortuous cracking path, also some snapped aggregate and the higher energy was required for overcoming interfacial bond (Chen and Liu, 2004). Especially for FA-ECC mixtures, rougher fracture surfaces were observed for ECC matrixes with maximum aggregate size of 1 mm. From the fractured surface, it was also observed that when the maximum aggregate size was small (0.4 mm for this study), the fracture surface of ECC matrix was smooth. While at high strength (for example ECC with slag), this effect was not as pronounced as in the low-strength matrix mixtures since the quality and porosity of the interfacial zone and matrix was greatly improved. At the range of the aggregate amount studied in this study, thus, more cracks passed through the aggregates in the case of high strength ECC (slag-ECC) while the effects of aggregate on bonding, deflecting and bridging cracks decreased.

4.3 Flexural Performance

The direct tensile test is considered to be the most accurate and effective method to confirm the strain-hardening behavior of a composite, as quasi-brittle fiber reinforced composites can potentially show apparent strain-hardening behavior under flexural loading, depending on the specimen geometry. However, one of the principle concerns in designing concrete structures is the flexural performance of the concrete. Flexural strength test of ECC is also an indirect measure of direct tensile performance. Therefore it was decided to use four-point bending test to investigate the flexural strength and ductility by measuring mid-span beam deflection capacity of ECC mixtures. Previous studies also demonstrate that deflection capacity can be correlated with the tensile strain capacity when the material shows truly strain hardening behaviour (Qian and Li, 2007; Qian and Li, 2008).

The test results in terms of flexural strength (modulus of rupture – MOR) and ultimate mid-span deflection at the peak stress are displayed in Table 4.3, and the

typical flexural stress-mid-span deflection curves for different aggregate amounts of the ECC mixtures are shown in Figure 4.3. To facilitate the comparison between the test results for different ECC mixtures, the same scales for both axes were used in these figures. In the flexural load–deflection curves, the stress at the first drop associated with the first cracking is defined as the first cracking strength, the maximum stress is defined as the flexural strength (modulus of rupture), and the corresponding deflection is defined as the flexural deflection (mid-span beam deflection) capacity. The flexural performances of ECC mixtures were calculated by averaging the results of six four-point bending measurements. It is important to note that the coefficient of variations of the flexural strength test results within each mix design is lower than 10%.

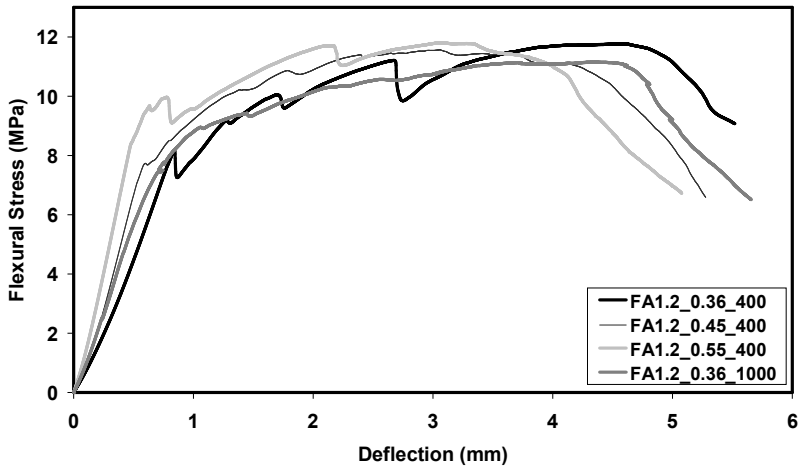

ECC with FA

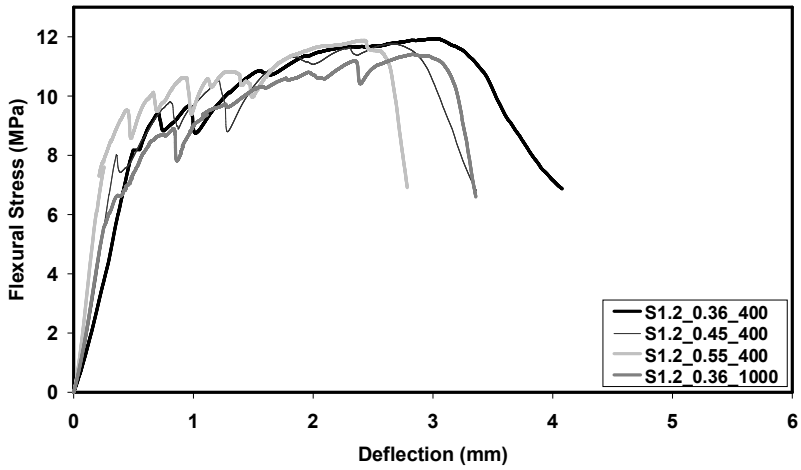

ECC with Slag

Figure 4.3. Typical flexural stress – mid-span deflection curves of ECC mixtures at age of 28 days

Table 4.3 Flexural strength test results of ECC mixtures

Mix ID.	Deflection, mm				Flexural Strength, MPa			
	7 d.	28 d.	90 d.	180 d.	7 d.	28 d.	90 d.	180 d.
FA1.2_0.36_400	5.68	4.83	4.49	4.41	8.48	12.73	12.80	12.91
FA1.2_0.45_400	4.52	4.23	3.99	3.81	7.51	11.92	12.19	12.59
FA1.2_0.55_400	4.09	3.97	3.84	3.71	7.69	11.41	12.42	12.87
FA1.2_0.36_1000	5.11	4.59	4.12	3.98	7.88	11.63	12.04	12.44
FA1.2_0.45_1000	4.38	4.14	3.79	3.67	7.96	11.12	11.98	12.18
FA1.2_0.55_1000	3.54	3.15	3.07	3.01	8.52	12.17	12.62	12.93
FA2.2_0.36_400	7.02	5.89	5.29	5.18	7.36	10.19	11.58	11.64
FA2.2_0.45_400	6.25	5.56	4.85	4.74	7.04	10.79	11.23	11.78
FA2.2_0.55_400	5.40	4.99	4.88	4.64	7.26	10.14	10.03	11.01
FA2.2_0.36_1000	5.55	4.72	4.50	4.40	6.59	9.39	10.59	11.17
FA2.2_0.45_1000	5.47	4.50	4.17	4.16	7.28	10.27	10.96	11.83
FA2.2_0.55_1000	4.73	4.02	3.92	3.72	7.14	9.35	10.13	10.94
S1.2_0.36_400	3.73	3.10	3.04	2.88	9.92	12.58	12.63	12.71
S1.2_0.45_400	3.24	2.71	2.62	2.49	9.89	12.38	12.70	12.98
S1.2_0.55_400	2.62	2.44	2.42	2.29	9.23	12.19	12.24	12.66
S1.2_0.36_1000	3.60	2.94	2.74	2.61	9.78	12.04	12.36	12.87
S1.2_0.45_1000	2.93	2.10	1.75	1.66	9.55	12.68	12.90	13.07
S1.2_0.55_1000	2.51	2.14	1.71	1.66	9.11	12.50	12.51	12.87
S2.2_0.36_400	4.31	3.98	3.44	3.31	8.44	11.50	11.78	12.02
S2.2_0.45_400	3.66	3.22	3.18	2.95	8.69	11.89	11.73	12.11
S2.2_0.55_400	3.23	2.55	2.21	2.05	8.45	11.42	11.35	11.63
S2.2_0.36_1000	4.14	3.35	3.06	2.77	8.63	11.29	11.15	11.47
S2.2_0.45_1000	3.55	3.10	2.73	2.60	8.73	11.73	11.46	11.88
S2.2_0.55_1000	3.01	2.30	2.16	1.95	8.82	11.58	11.82	12.13

4.3.1 Load-deflection curves

Typical load deflection curves for PVA-ECC incorporating 2 percent volume fraction of PVA fibers, different amount of aggregate content and MAS were presented in Figure 4.3 for comparison. As seen from the figure, under severe bending load, an ECC beam containing aggregate up to 1.0 mm MAS deforms similarly to a ductile metal plate through plastic deformation (Figure 4.4). Each specimen was examined using a portable microscope during and after the loading to determine the crack width and distribution. In all ECC specimens, the first cracks to appear were flexural cracks starting at the surface of the tension face. After first cracking, the load continues to rise accompanied by multiple cracking, which contributes to the inelastic deformation as stress increases. Shortly after initial cracking, the crack width grows rapidly with an increase of deformation, and then stabilizes at a value between 40 to 90 μm while additional micro-cracks further develop. Microcracks developed from the first cracking point and spread out in the mid-span of the flexural beam as shown in Figure 4.4. Bending failure in ECC occurred when the fiber bridging strength at one of the microcracks was reached, resulting in localized deformation at this section (Figure 4.4) once the flexural strength is approached.

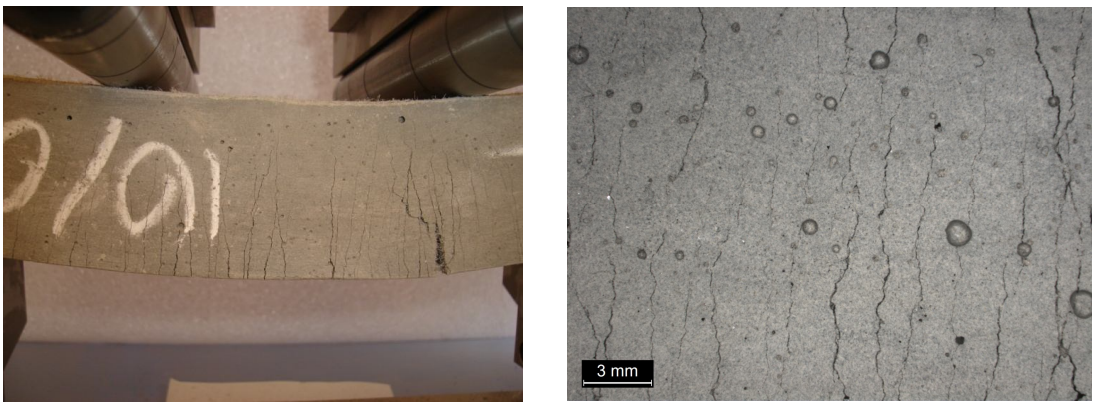

Figure 4.4 Typical cracking patterns of ECC beam specimen after flexure load applications (Mix ID.: FA1.2_0.55_1000)

The first crack strength was defined as the strength at which the strength-deformation response deviated from linearity. The average first crack strengths of ECC mixtures vary from 6.0 to 8.0 MPa in accordance with mineral admixture type (FA or slag) and replacement rate. The increase in FA (or S)/C ratio from 1.2 to 2.2 reduces the

first crack strength by an average of up to 20 percent. However, aggregate amount and MAS had little or no influence on the magnitude of the first crack loads of the ECC beams at constant mineral admixture replacement rate. The slope of the load-deflection curve represents the stiffness of the beams and it can be easily noted from Figure 4.3 that the slope increases significantly with replacement of slag and increasing aggregate content, and thereby indicating an increase in the stiffness of the ECC beams. This result is consistent with what is stated in the literature (Aïtcin and Mehta, 1990; Baalbaki et al., 1991; Cetin and Carrasquillo, 1998). Aggregate is known to be stiffer than mortar, the other component of ECC. Thus, inclusion of higher aggregate content makes the final product stiffer. As also shown in Figure 4.3, ECC with 0.4 or 1.0 mm maximum aggregate size had very similar stiffness for ECC mixtures containing same mineral admixture (FA or slag) and at all aggregate content levels. As a result, within the size range studied, elastic modulus appears to be independent of MAS at a given aggregate content. This observation makes sense because; stiffness measurements were performed using the initial slopes of the load-deflection curves (generally up to 40 percent of the ultimate load). Bond strength is not likely to be a dominant factor to influence the test result at this load level (Cetin and Carrasquillo, 1998).

4.3.2 Flexural strength (modulus of rupture – MOR)

The flexural strength values are summarized in Table 4.3. As seen from Table 4.3, the average ultimate flexural strengths vary from 9.35 to 12.73 MPa at 28 days of age. Specimens which contained slag consistently developed slightly higher strength than specimens of identical mix proportions, but contained FA especially at the ages of 7 days, however similar values at later ages. It is also apparent that different from the compressive strength test results there is not a significant influence of the FA or slag replacement rate on the flexural strength values especially at the ages of 28 days or later in the tested range. For example, the flexural strength of ECC with FA/C ratio of 2.2 is about 85% that of the ECC mixtures with FA/C ratio of 1.2. This value is about 93% that of ECC mixtures with S/C ratio of 1.2. The MOR is likely limited by the fiber bridging capacity governed by the fiber/matrix bond and in turn by the mineral admixture replacement rate. However, even at about 70% replacement of cement by FA or slag (mineral admixture / cement ratio of 2.2), the flexural strength

of ECC at 28 days was significantly higher than that of conventional concrete and fiber reinforced concrete. Moreover, flexural strength increased with age more slowly than compressive strength. As in the case of compressive strength test results, the aggregate content and MAS had also no or only a minor effect on the flexural strength.

4.3.3 Mid-span beam deflection

The flexural deflection capacity of ECC mixtures, which reflects the material ductility, with different FA and slag contents, aggregate size and amount are summarized in Figure 4.5 and Table 4.3. As shown in Figure 4.5, the total deflection of ECC beam strongly depends on the type and amount of mineral admixture. The mixes of slag-ECC showed significantly lower deflection capacity when compared to the ductility of the mixes of FA-ECC. The reduced ductility can possibly be caused by the higher fracture toughness, bond strength and friction between the slag-ECC matrix and the fibers compared with FA-ECC. The microstructural studies provide some assistance in evaluating the differences in macroscopic behavior between FA-ECC and slag-ECC. The SEM observation was made with specimens at the age of 28 and 180 days, respectively. The SEM observation of slag-ECC also showed that microstructure changed greatly with the incorporation of slag, and no unhydrated particles could be observed. The increase in fiber/matrix frictional bond strength with an addition of slag was also verified with SEM image observations (Figure 4.6), which may be detrimental to achieving sufficient multiple cracking and strain-hardening behavior. Differences in the matrix surrounding a fiber are seen between specimens containing FA and slag. Comparing Figure 4.6(a) with Figure 4.6(b), the fiber surfaces in slag-ECC have more attached matrix material compared to FA-ECC. For a fiber to be pulled out of the slag-ECC matrix, de-bonding at the fiber-interface or fracture of the hydrate product is required to overcome interlocking of the hydrate product (Gao and Van Zijl, 2004). Although slag-ECC mixtures exhibit smaller deformation capacity, their flexural deflection capacity is around or more than 2 mm at 28 days of age. The 2.0 mm deformation is nearly equivalent to 1.5% strain capacity on the tensile face of the beam. This deflection capacity remains almost 150 times higher than that in normal concrete and conventional fiber reinforced concrete.

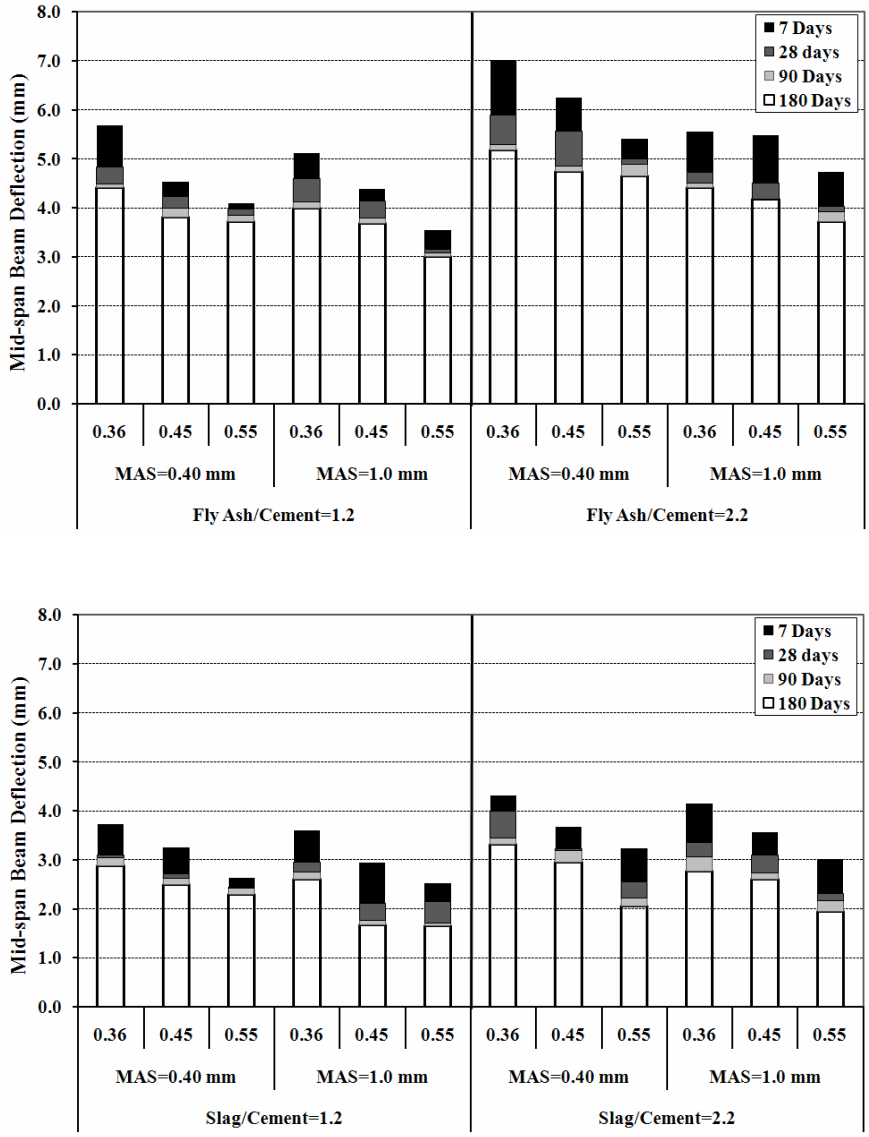

Figure 4.5 The influence of mineral admixture, aggregate size and amount on the deformability in flexure

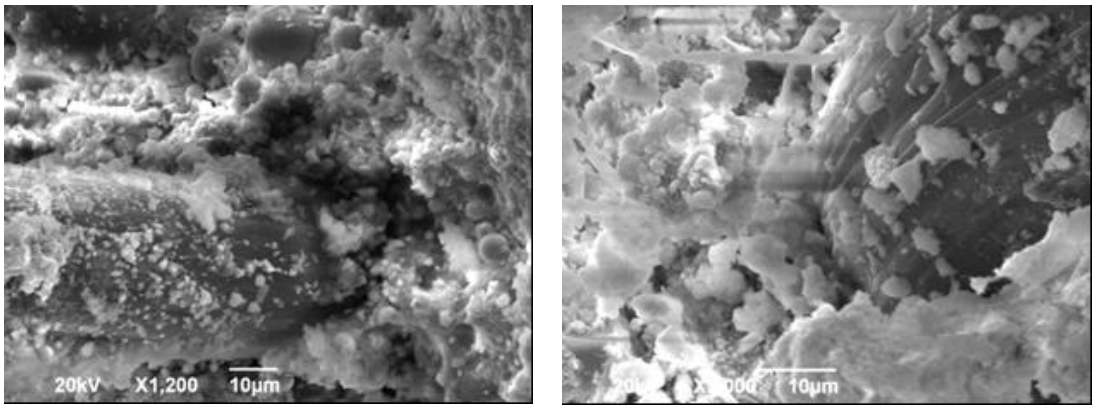

(a) FA-ECC **(b) Slag-ECC**

Figure 4.6 SEM image from the fractured surface

From Figure 4.6, a trend of increased deformability – ductility – with mineral admixture content (FA or slag) beyond 55% could be detected. This effect was more pronounced in FA-ECC mixtures. The total deflection increased as the replacement level of FA increases, reaching as much as 7.02 mm at peak load at the ages of 7 days. The 7.02 mm deformation is more than 4% strain capacity on the tensile face of the beam. The deformation capacity measured after 7 days was lower than the 7-day deformation capacity for all ECC mixtures. However, the overall effect of this slight drop in long-term deformation capacity was minimal. Based on the similarity of test results up to 180 days, the flexural deformation capacity seemed to stabilize after 28 days. The time dependent deformation capacity change described above has been known for sometime and is ascribed to the increase in fiber/matrix interface properties and matrix toughness associated with the continued hydration process of binder (Wang and Li, 2007; Şahmaran and Li, 2009). Figure 4.6(a) shows that there are numerous un-hydrated spherical FA particles in the interfacial zone of FA-ECC mixtures both at the age of 28 and 180 days. It is apparent that the fiber was pulled out from the matrix, leaving a smooth interfacial surface. This is in agreement with the widely acknowledged fact that FA content beyond 30-40% does not participate in the hydration process, but could be seen as mere filler material, or aggregate. Thus, delayed hydration of FA did not set in and reduce the effective slippage mechanism in FA-ECC, which can also be clearly seen from Figure 4.5. In addition to fiber-pull-out from the matrix from during flexural loading, the presence of unhydrated FA particles decreased matrix toughness and contributes to the crack pattern and eventual tortuous crack path of the localized, failing crack (Gao and Van Zijl, 2004). The use of FA is also expected to provide benefits in terms of improving the fiber dispersion, which is associated with enhanced workability. Therefore mineral admixture type, its chemical composition and physical and morphological properties play key roles in the resultant composite performance.

Adverse effects of increased size of aggregates on ductility performances of ECC are shown in Figure 4.5. This figure indicated that the increase in aggregate size and amount up to a certain volume fraction and 1 mm size results in a decrease in the ductility characteristics, total mid-span beam deflection, of ECC. Test results also show that FA tend to perform significantly better than slag even at higher aggregate amount and sizes and was not affected to the same extent as those of slag-ECC

mixtures. When the FA/C ratio was increased from 1.2 to 2.2, ECC mixtures with higher amount of aggregate and larger MAS showed higher deflection capacity to that of standard ECC beams (FA1.2_0.36_400, M45). The negative effects of increasing aggregate size at large aggregate content on ductility may be attributed to the corresponding damage to the uniform dispersion of fibers. The balling of fibers encouraged by coarser aggregates at constant aggregate content prevents sufficient coating of fibers by the matrix, and thus reduces the fiber-to-matrix bonding, which is an important factor influencing ductility (Soroushian et al.,1992). Moreover, for ECC with the larger aggregate size and volume, a higher degree of aggregate interlock is expected, resulting in higher matrix toughness and work-of-fracture during crack propagation. According to the micromechanical model of steady state cracking, which is essential to achieving strain hardening behavior, high matrix fracture toughness reduces the margin to develop multiple (Li et al., 1995; Li, 1997). The relationship between the fracture toughness and mid-span beam deflection value obtained from four-point bending test is shown in Figure 4.7. From these results, notice that the deflection is almost inversely proportional with the fracture toughness (an inverse linear correlation constant of 0.86).

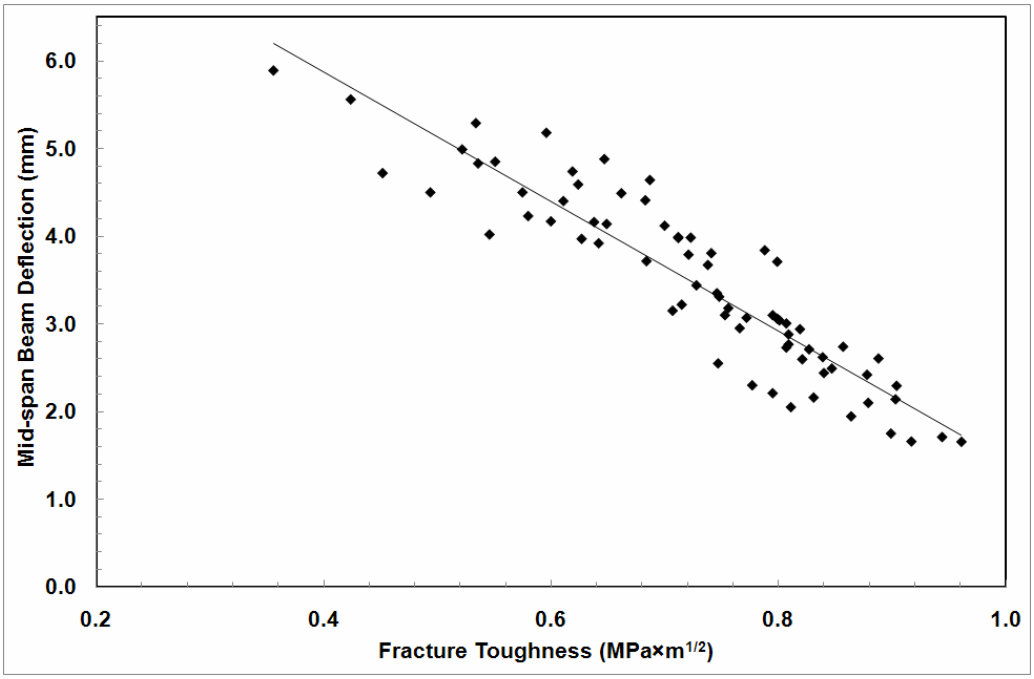

Figure 4.7. Correlation between fracture toughness versus mid-span beam deflection

4.3.4 Crack characterization

After unloading, multiple microcracks with a small average crack width, fine crack spacing and different amount of flexural strength tests were observed on all ECC specimens tested under flexural loading. With crack width measurement on the surface of the specimens, it has been indicated that average crack width was lower than 90 μm in average for slag-ECC mixtures and 70 μm in average for FA-ECC mixtures. At the age of 180 days, this width has been reduced to lower than 70 μm by increasing the slag-cement ratio from 1.2 to 2.2. It was also found that the crack width reduces significantly as FA content increased at all ages. At the age of 180 days, the residual crack width of ECC mixtures with FA/C ratio of 2.2 was about 40 μm with smaller crack spacing. The reason for this is not completely clear, but is likely associated with the enhanced fiber slippage due to spherical shaped FA particles along the fiber-matrix interface and more uniform distribution of fibers throughout the matrix. On the other hand, the use of aggregate up to 1.00 mm MAS and 0.55 aggregate/binder ratio did not influence the average residual crack width. Crack width control is of primary importance for many reinforced concrete applications, since it is believed that there is a close relationship between the mean or maximum crack widths and the durability of the structure (Lepech and Li, 2005; Şahmaran and Li, 2009a). Water flow, or permeability, is proportional to crack width cubed, which means ECC with multiple smaller cracks is less permeable than that with one large crack. Moreover, the lower magnitude of the crack width is expected to promote the self-healing behavior, and thus the transport properties in cracked composites (Yang et al., 2005; Lepech and Li, 2005; Şahmaran et al.,2007; Şahmaran and Li, 2009b). Consequently, in the serviceability limit state a mean or maximum crack width less than about 0.1 mm is usually prescribed (Evardsen, 1999; Reinhardt and Jooss, 2003).

4.4 Drying Shrinkage

This section of the thesis presents the results of the free drying shrinkage tests. The effects of MAS, aggregate amount, and mineral admixture type and replacement rate on the free shrinkage of ECC mixtures are evaluated with the goal of establishing guidelines to reduce cracking in ECC. The free drying shrinkage specimens were

stored in a controlled environment at 23 ± 2°C and 50 ± 4 percent relative humidity, and free shrinkage was recorded as the change in length over a gage length (distance between tips of gage studs) of 254 mm up to a period of 180 days. The results of drying shrinkage test at the age of 180 days are shown in Figure 4.8. Each value in Figure 4.8 represents the average drying shrinkage measurements of three specimens. The ECC mixtures produced for this study had the same W/CM ratio, so varying water requirement was not a factor for drying shrinkage.

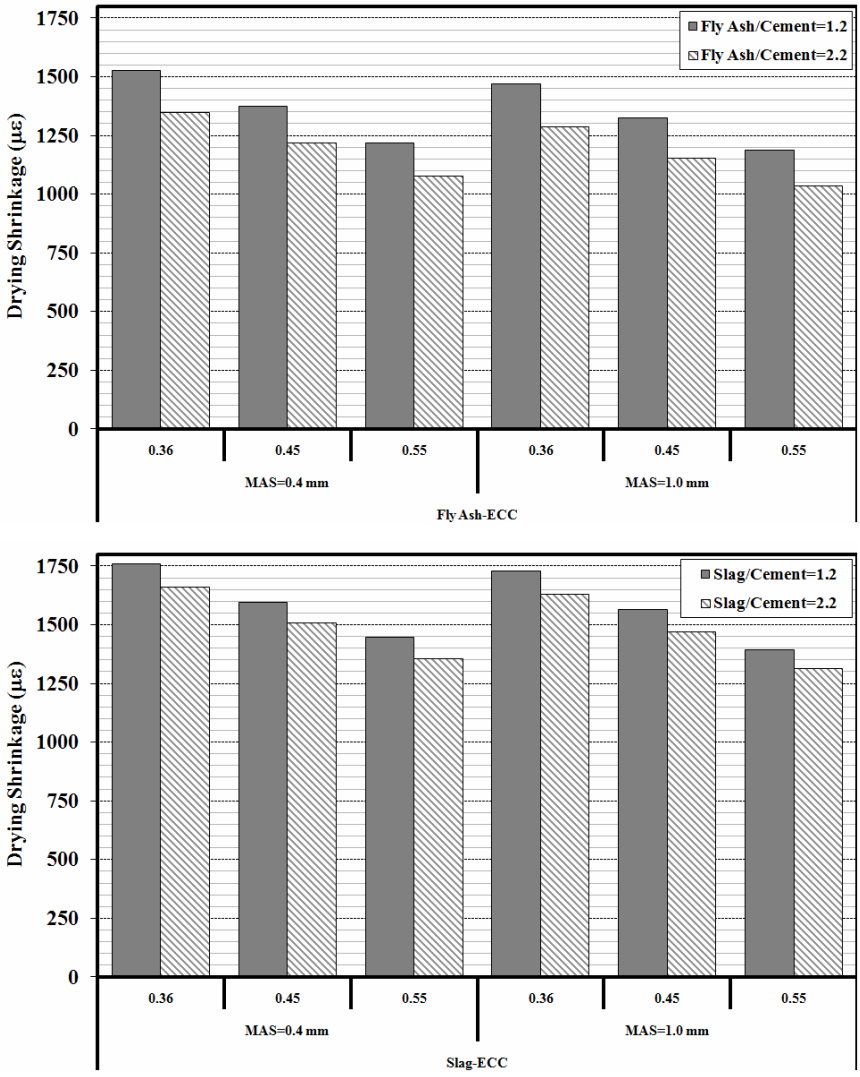

Figure 4.8 Drying shrinkage of ECC mixtures at 180 days

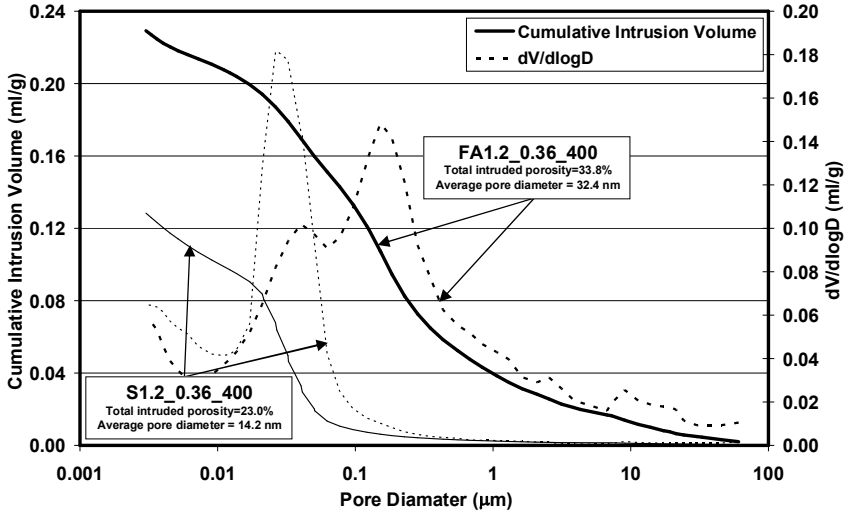

Figure 4.9 Comparison of pore size distribution of ECC mixtures with FA and slag at 28 days

The drying shrinkage strains at the age of 180 days ranged between 1035 and 1761 micro-strain. ECC mixtures with S/C ratio of 1.2, aggregate/binder ratio of 0.36 (the lowest aggregate content) and MAS of 0.4 mm (S1.2_0.36_400) exhibited the highest drying shrinkage of 1761 με at the end of 180 days. The general trend in Figure 4.8 shows that the increase in the mineral admixture content, especially FA, can effectively reduce free drying shrinkage deformation. Similar results have been reported for HVFA concrete (Şahmaran et al.,2007; Şahmaran et al.,2009). In the present study, a reduction between 11 to 13% of drying shrinkage depending on the aggregate size and amount was found when the FA/C ratio was increased from 1.2 to 2.2. A possible mechanism contributing to the reduction of drying shrinkage in ECCs is the matrix densification due to FA addition, which may prevent internal moisture evaporation (Maslehuddin et al., 1987). The matrix densification is typically attributed to the shape, pozzolanic property, and micro-filler effect of FA. An alternative mechanism is that unhydrated FA particles act as aggregates, which provide restraint to shrinkage, and the coarser pore structure, which results in decreased surface tension when a meniscus is formed and, thus, lower shrinkage forces exerted on the surrounding cement paste (Bisaillon et al., 1994; Zhang, 1995; Şahmaran et al.,2007). On the other hand, compared with FA-ECC mixtures, the use of partial volume replacement of portland cement by slag without changing the MAS or aggregate content can lead to increase ultimate drying shrinkage between 15 to 27%. For example, mix S1.2_0.36_400 has similar mixture proportions as mix

FA2.2_0.55_1000, while the shrinkage strain of mix S2.2_0.55_1000 at the age of 180 days is 1315 με, which is more than 27% higher than that of FA2.2_0.55_1000. The increase in the drying shrinkage of ECC might be due mainly to pozzolanic reaction and enhanced pore size refinement mechanism of slag especially at earlier ages. Typical pore size distribution curves are shown in Figure 4.9 for the FA-ECC and slag-ECC mixtures. As seen in Figure 4.9, the porosity of slag-ECC was much lower and has finer sizes than FA-ECC, which may proportionately increase free shrinkage. The total porosity and average pore diameter increased with an increase in the replacement of mineral admixture content. It was also observed that for a given aggregate content and size, a reduction up to 6% of drying shrinkage was found when the slag/C ratio was increased from 1.2 to 2.2.

It is clear from this experimental study that the effect of aggregate content was more pronounced than that of the aggregate size on the long-term drying shrinkage. Each 0.10 rate increase in the aggregate/binder ratio decreased the value of shrinkage in the order of almost 10%. This trend was consistent with different mineral admixture types and replacement rates. Shrinkage was lowest with the highest aggregate content (aggregate/binder ratio of 0.55). This is attributed, not only to the restraint provided by aggregates to shrinkage, but also to the reduction in paste content with the increase in aggregate content. Aggregates can also play the role of microcrack-arrestors in the matrix, further improving the composite behavior. On the other hand, for the range of maximum sizes from 0.4 mm to 1 mm studied, the differences in drying shrinkage were so small as to be of little practical significance in most concrete applications.

The interference of aggregates with fiber dispersion, which tends to be more pronounced at higher volume fractions of larger aggregates (1 mm for this study), however, can reduce the composite performance. This effect is discussed in previous section to cause a reduction in flexural deflection capacity with increasing volume fraction of larger aggregates in ECC with 2 percent PVA fiber volume fraction. At such relatively moderate fiber volume contents, therefore, the negative effects of larger amount and size of aggregate on fiber dispersion, matrix and interface properties, and thus flexural ductility seem to be compensated by the positive effects

of aggregates on the dimensional stability of ECC mixtures, especially when incorporating FA.

4.5 Restrained Shrinkage Cracking

Shrinkage cracking is a major problem for concrete structures, especially for flat structures, such as highway pavement, slabs and walls. Free shrinkage tests alone cannot offer sufficient information on the behavior of concrete structures because virtually every concrete structure is restrained in some way, either by reinforcement or by the boundary condition of the structure. In this study, the method of the ECC ring cast next to a steel ring is used to simulate restrained shrinkage cracking. The ring specimens provide a simple test method in which the effect of restrained shrinkage cracking can be easily studied. Under the effect of restrained shrinkage, tensile stresses are developed. When they are greater than the tensile strength of the ECC mixtures, a crack appears. When a crack is formed in ECC, fibers that bridge the crack prevent it from opening more. With the action of shrinkage, fibers transmit forces through the crack and thus create tensile stresses along the ring (Mesbah and Buyle-Bodin, 1999). Since loads transmitted by fibers are high enough, as in ECC, then the second crack will form because the tensile stress transmitted across the crack is larger than the tensile strength of the matrix. Experimental results obtained in restrained shrinkage test confirm this tendency.

The typical development of an average crack width with time for restrained shrinkage specimens is shown in Figure 4.10. All of the ECC mixtures showed some degree of multiple cracking. Basically, the width of a crack developed very fast in the first few days after crack formation. From then on the rate of development diminished its intension or stabilized. Figure 4.10 shows that slag-ECC mixtures began to crack after 3 to 4 days, and FA ECC mixtures after 4 to 9 days in accordance with mineral admixture replacement rate and aggregate amount. The benefit of using FA was immediately obvious in the observed increase in the age of restrained shrinkage cracking (when compared with the mixture containing slag). In addition, the creation of the first crack was significantly delayed in time with an increase in aggregate content. The total crack widths for all the FA-ECC mixtures were significantly smaller than the cracks developed in slag-ECC mixtures. On

increasing the volume of FA, further improvements were obtained in the potential for restrained shrinkage cracking behavior. On the other hand, the crack onset time was accelerated and the crack width was increased for slag-ECC specimens, and was not affected with the increase the volume of slag. As seen from Figure 4.10, the use of slag led to not only higher ultimate shrinkage capacity (as discussed in previous section) but also higher early age shrinkage. The higher early age shrinkage could lead to significant cracking because of low tensile strength of ECC at early age.

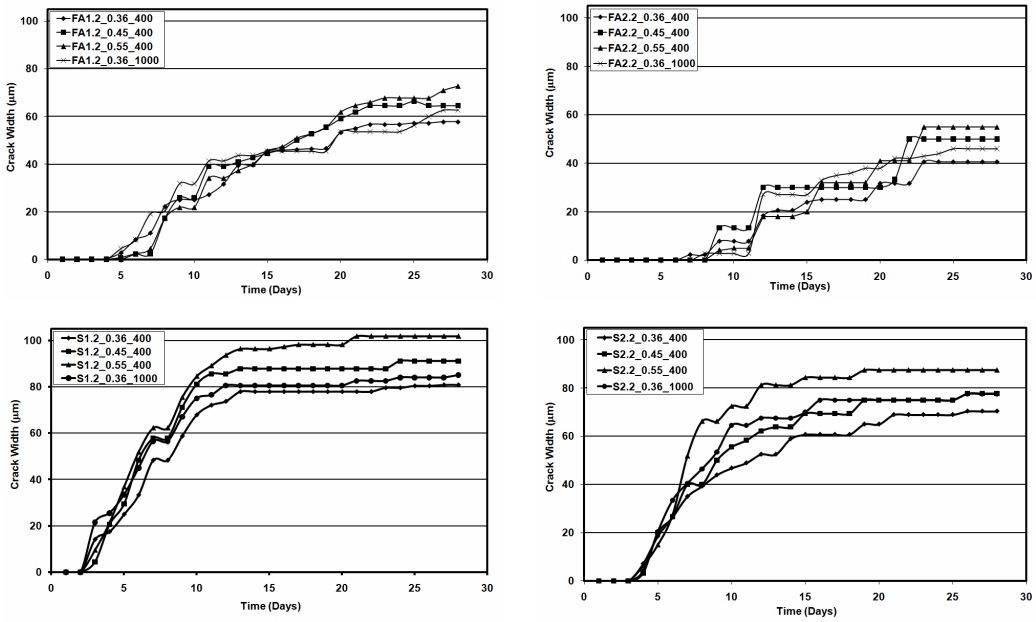

Figure 4.10 Development of crack width in restrained specimens with time

CHAPTER V

CONCLUSIONS

This thesis described the influence of aggregate size and amount on the mechanical performances and dimensional stability of ECC with mineral admixture. ECC mixtures contain mineral admixture (fly ash or slag) with mineral admixture/cement ratio of 1.2 or 2.2, aggregate with maximum grain sizes of 0.4 or 1.0 mm and aggregate/binder ratio of 0.36, 0.45 and 0.55. For comparison purpose, standard ECC mixture with FA/C ratio of 1.2, micro silica sand with an aggregate to binder ratio (A/B) of 0.36 (Mix. ID: FA1.2_0.36_400 – M45) were also produced. The following conclusions can be drawn from this study.

1. Increase in mineral admixture (FA and slag) replacement rate lead to a reduction in fracture toughness of matrix, and compressive and flexural strengths of composites whereas ductility increases. The ECC ductility, by measuring mid-span beam deflection capacity, strongly depends on the type and amount of mineral admixture. The mixture of slag-ECC showed significantly lower deflection capacity when compared to the ductility of the mixture of FA-ECC. The reduced ductility can possibly be caused by the higher fracture toughness, matrix and bond strength and friction between the slag-ECC matrix and the fibers compared with FA-ECC mixtures.

2. For a given mineral admixture type and content, fracture toughness of specimens produced without PVA fiber significantly affected while there was no definite change in compressive and flexural strength as aggregate size and amount increases. Moreover, increase in the percentage of aggregate size and its amount, adversely influenced ductility of ECC specimens. The ductility of ECC could be improved through the addition of coarse aggregate with the quantity more than used in the standard ECC mixture. This was true as long as the maximum size and content of aggregates did not exceed certain limits, beyond which aggregates start to increase

matrix fracture toughness to a limit value, interfere with the uniform dispersion of fibers and negatively influence the composite ductility. The negative effects of aggregates on fiber dispersion were particularly pronounced in composites with lower mineral admixture replacement rate (especially slag) when relatively large contents of coarser aggregates (1 mm MAS for this study) are used. The negative effects of aggregates on fiber dispersion and matrix toughness can be eliminated or minimized by increasing mineral admixture content (replacing cement). In this study, the FA-ECC mixtures produced with higher maximum aggregate sizes and amount exhibit strain-hardening behavior with deformation capacities better than the standard ECC mixtures. This was true for all aggregate amount and sizes used in the production of ECC in this study.

3. There is a strong correlation between the deflection capacity and the matrix fracture toughness. As the matrix fracture toughness decreases, the deflection capacity increases.

4. After unloading, multiple microcracks with a small average crack width, fine crack spacing and different amount were observed on all ECC specimens tested under flexural loading. With crack width measurement on the surface of the specimens, it has been indicated that average crack width was lower than 90 μm in average for slag-ECC mixtures and 60 μm in average for FA-ECC mixtures. In slag ECC, cracks were also spaced further apart than in FA-ECC. On the other hand, the use of aggregate up to 1.00 mm MAS and 0.55 aggregate/binder ratio did not influence the average residual crack width. Crack width control is of primary importance for many reinforced concrete applications, since it is believed that there is a close relationship between the mean or maximum crack widths and the durability of the structure.

5. Cement replacement with FA and increase in aggregate content have a significant influence on the drying shrinkage and restrained shrinkage cracking when compared with the slag-ECC. The ultimate drying shrinkage and restrained shrinkage cracking performance of ECC further improve with further increase in the FA content. Test results also suggests that, within the limited aggregate size employed in the present experiments, no significant role of size of aggregate on the ultimate shrinkage is

observed for a given aggregate content. The ultimate drying shrinkage of ECC slightly decreases with increase in the size of aggregate from 0.4 mm to 1.0 mm. In comparison, ECC with identical replacement of cement with slag resulted in significantly higher drying shrinkage and a decrease in the age of restrained shrinkage cracking.

Finally, the results presented in this study provide a preliminary database for the suitability of locally available aggregate in the production of ECC, and indicate that locally available aggregate with relatively higher nominal aggregate size and aggregate amount can also be successfully used to produce an ECC having similar or better mechanical properties than corresponding ECC made with micro-silica aggregate. These conclusions are confined to the ECC defined herein, and are based on the experimental results described in this study.

REFERENCES

ACI Committee 116R. (1994). *Cement and concrete terminology*. ACI manual of concrete practice.

ACI Committee 224R. (2001). *Control of Cracking in Concrete Structures*. American Concrete Institute, Farmington Hills, Michigan.

ACI Committee 318R (2002). *Building Code Requirements for Structural Concrete and Commentary.* American Concrete Institute, Farmington Hills, Michigan, pp. 443

Aïtcin, P.C. and Mehta, P.K. (1990). Effect of Coarse Aggregate Characteristics on Mechanical Properties of High-Strength Concrete. *ACI Materials Journal*, **87** 103-107.

ASTM Standard C39. (2003). *Standard test method for compressive strength of cylindrical concrete specimens.* American society for testing and materials. West Conshohocken, PA, USA.

ASTM Standard C157. (2004). *Test method for length change of hardened hydraulic cement mortar and concrete.* American society for testing and materials. West Conshohocken, PA, USA.

ASTM Standard C618. (2003). *Standard specification for coal fly ash and raw or calcined natural pozzolan for use in concrete.* American society for testing and materials. West Conshohocken, PA, USA.

ASTM Standard C 666. (1991). *Standard Test Method for Resistance of Concrete to Rapid Freezing and Thawing.* American Society for Testing and Materials, Philadelphia, USA.

ASTM Standard C 672. (2001). *Standard Test Method Scaling Resistance of Concrete Surfaces Exposed to De-icing Chemicals.* American Society for Testing and Materials, Philadelphia, USA.

ASTM Standard C989. (2009). *Standard specification for slag cement for use in concrete and mortars.* American society for testing and materials. West Conshohocken, PA, USA.

ASTM Standard C1260. (1994). *Standard Test Method for Potential Alkali Reactivity of Aggregates (Mortar-bar method).* In: Annual book of American Society for Testing and Materials, Philadelphia, USA.

ASTM Standard E399. (2003). *Test method for plane-strain fracture toughness of metallic materials.* American society for testing and materials. West Conshohocken, PA, USA.

Baalbaki, W., Benmokrane, B., Chaallal, O. and Aïtcin, P.C. (1991). Influence of Coarse Aggregate on Elastic Properties of High Performance Concrete. *ACI Materials Journal*, 499-503.

Bakker, R.F.M. (1988). Initiation period of corrosion. *RILEM Report: Corrosion of Steel in Concrete edited by P. Schiessl*, pp. 22-55.

Beeldens, A. and Vandewalle, L. (2001). *Durability of high strength concrete for highway pavement restoration.* CONSEC 01: Third International Conference on Concrete under Severe Conditions, Vancouver, BC, Canada, pp. 1230-1238.

Bisaillon, A., Rivest, M. and Malhotra, V.M. (1994). Performance of high-volume fly ash concrete in large experimental monoliths. *ACI Materials Journal*, **91,** 178-187.

Carlson, R.W. and Reading, T.J. (1988). Model study to shrinkage cracking in concrete building walls. *ACI Materials Journal,* **85,** 395–404.

Cetin, A. and Carrasquillo, R.L. (1998). High-performance concrete: Influence of coarse aggregates on mechanical properties. *ACI Material Journal,* **95,** 252–261.

Chang, P.K., Peng, Y.N. and Hwang, C.L. (2001). A design consideration for durability of high-performance concrete. *Cement and Concrete Composites*, **23,** 375-380.

Chen, B. and Liu, J. (2004). Effect of aggregate on the fracture behavior of high strength concrete. *Construction and Building Materials*, **18**, 585- 590.

Davis, D.E. and Alexander, M.G. (1989). Properties of Aggregate in Concrete (Part 1). *Hippo Quarries, Sandton, South Africa: Hippo Quarries Technical Publication.*

Davis, D.E.and Alexander M.G. (1992). Properties of Aggregate in Concrete (Part 2). *Hippo Quarries, Sandton, South Africa: Hippo Quarries Technical Publication*.

De Larrard Francois and Belloc Albert. (1997). The influence of aggregate on the compressive strength of normal and high-strength concrete. *ACI Material Journal,* **94,** 417–25.

Evardsen, C. (1999). Water permeability and autogenous healing of cracks in concrete. *ACI Materials Journal*, **96,** 448-454.

Federal Highway Administration (FHWA). (1992). *Corrosion Detection in Reinforced Concrete Bridge Structures*, Project 84, Washington, DC.

Fischer, G.S. W. and Li, V.C. (2003). Design of Engineered Cementitios Composites (ECC) for Processing and Workability Requirement. In: BMC 7, Poland, pp. 29-36.

Gao, Song and Van Zijl, G.P.A.G. (2004). Tailoring ECC for commercial application. In: M. di Prisco, R. Felicetti and G.A. Plizzari, Editors, *Fibre-Reinforced Concretes (BEFIB'2004), RILEM Pro039*, pp. 1391–1400.

Gerard, B., Reinhardt, H.W. and Breysse, D. (1997). Measured transport in cracked concrete. *Penetration and Permeability of Concrete: RILEM Report 16, Ed. H.W. Reinhardt*, pp. 265-331.

Glasser, F.P. (1991). Chemical, Mineralogical, and Microstructural Changes Occuring in Hyrated Slag-Cement Blends. *Materials Science of Concrete II,* The American Ceramic Society, Inc., Loc., pp. 41-81.

Haque, M.N., Kayyali, O.A. and Gopalan, M.K. (1992). Fly Ash Reduces Harmful Chloride Ions in Concrete. *ACI Materials Journal*, **89,** 238-241.

Hearn, N. (1999). Effect of shrinkage and load-induced cracking on water permeability of concrete. *ACI Materials Journal,* **96,** 234-241.

Hogan, F.J. and Meusel, J.W. (1981). Evaluation for Durability and Strength Development of a Ground Granulated Blast- Furnace Slag, Cement, Concrete, and Aggregates, **3,** 40-52.

Hwang, C.L., Liu, J.J., Lee, L.S. and Lin, F.Y. (1996). Densified Mixture Design Algorithm and Early Properties of High Performance Concrete. *Chinese Institute of Civil and Hydraulic Engineering,* **8,** pp. 217-229.

Inaguma, H., Seki, M., Suka, K. and Rokugo, K. (2005). Experimental study on crack-bridging ability of ECC for repair under train loading. *Proc. Of Int'l Workshop on HPFRCC in Structural Applications*, Honolulu, Hawaii, USA., pp. 499-508.

Kanda, T., Saito, T. and Sakata, N. (2003). Tensile and anti-spalling properties of direct sprayed ECC. *Advanced Concrete Technology*, **1,** 269-282.

Kim, Jin-Keun, Kim, Jeong-Su, Ha, Gee Joo and Kim, Yun Yong (2007). Tensile and fiber dispersion performance of ECC (engineered cementitious composites) produced with ground granulated blast furnace slag. *Cement and Concrete Research,* **37,** 1096–1105.

Kim, Y.Y., Kim, J.S., Kim, H.S., Kim, J.K. and Ha, G.J. (2004). *Uniaxial Tensile Behavior of High Ductile Fiber Reinforced Mortar Designed with Ground Granulated Blast Furnace Slag*. KSCE Conference, **1**, 546-551.

Kim, Y.Y., Kong, H.J. and Li, V.C. (2003). Design of Engineered Cementitious Composite (ECC) suitable for wet-mix shotcreting. *ACI Materials Journal,* **100,** 511-518.

Kong, H.J., Bike, S. and Li, V.C. (2003a). Development of a Self-Consolidating Engineered Cementitious Composite Employing Electrosteric Dispersion/Stabilization. *Journal of Cement and Concrete Composites*, **25,** 301-309.

Kong, H.J., Bike, S. and Li, V.C. (2003b). Constitutive Rheological Control to Develop a Self-Consolidating Engineered Cementitious Composite Reinforced with Hydrophilic Poly(vinyl alcohol) Fibers. *Journal of Cement and Concrete Composites,* **25,** 333-341.

Kosmatka, S.H. and Panarese, W.C. (1988). *Design and control of concrete mixtures*. Thirteenth ed. Portland Cement Association, Skokie, IL pp.205.

Kraai, P.P. (1985). Proposed test to determine cracking potential due to drying shrinkage of concrete. *Concrete Construction*, **30,** 775–778.

Kunieda, M. and Rokugo, K. (2006). Recent Progress on HPFRCC in Japan. *Journal of Advanced Concrete Technology,* **4,** 19-33.

Lepech, M. and Li, V.C. (2005). Water *Permeability of Cracked Cementitious Composites.* In: Proceeding of Eleventh International Conference on Fracture*,* Turin, Italy, pp. CD-Paper 4539.

Lepech, M. and Li, V.C. (2005). *Durability and Long Term Performance of Engineered Cementitious Composites*. In Proceedings of International RELIM Workshop on HPFRCC in Structural Applications, Honolulu, Hawaii, pp. 165-174.

Lepech, M. and Li, V.C. (2007). Large Scale Processing of Engineered Cementitious Composites. Accepted for publication in *ACI Materials Journal*, July 2007.

Li, M., Şahmaran, M. and Li, V.C. (2007). Effect of cracking and healing on durability of Engineered Cementitious Composites under marine environment. *HPFRCC 5 - High Performance Fiber Reinforced Cement Composites*, Stuttgart, Germany, pp. 313-322.

Lin, Z. and Li, V.C. (1997). Crack Bridging in Fiber Reinforced Cementitious Composites with Slip-Hardening Interfaces. *Journal of Mechanics and Physics of Solids,* **45,** 763-787.

Lin, Z., Kanda, T. and Li, V.C. (1999). On interface property characterization and performance of fiber reinforced cementitious composites. *Concrete Science and Engineering, RILEM,* **1,** 173-184.

Li, V.C. (1997). Engineered Cementitious Composites Tailored Composites Through Micromechanical Modeling in Fiber Reinforced Concrete: Present and the Future, Banthia, N. A., Bentur and Mufti, A. Editor. *Canadian Society for Civil Engineering*,pp. 64-97.

Li V.C. (1998). ECC tailored composites through micromechanical modeling. *Fiber Reinforced Concrete: Present and the Future edited by Banthia et al*, CSCE, Montreal, pp. 64-97.

Li, V.C. (2003). On Engineered Cementitious Composites (ECC) A Review of the Material and Its Applications. *Journal of Advanced Concrete Technology,* **1,** 215-230.

Li, V.C. (2006). Integrated Structures and Materials Design. *RILEM Journal of Materials and Structures,* 1-10.

Li, V.C. and Lepech, M. (2004). *Crack resistant concrete material for transportation construction.* In TRB 83rd Annual Meeting, Washington, D.C., Compendium of Papers CD ROM, pp. 04-4680.

Li, V.C. and Leung, C.K.Y. (1992). Theory of steady state and multiple cracking of random discontinuous fiber reinforced brittle matrix composites. *ASCE Journal of Engineering Mechanics*, **118,** 2246–2264.

Li, V.C. and Stang, H. (2004). *Elevating FRC material ductility to infrastructure durability*. Proceedings of BEFIB, Varenna, Lake Como, Italy, pp 171-186.

Li, V.C., Fischer, G., Kim, Y.Y., Lepech, M., Qian, S., Weimann, M. and Wang, S. (2003). *Durable link slabs for jointless bridge decks based on strain-hardening cementitious composites.* Report for Michigan Department of Transportation RC-1438.

Li, V.C., Horikoshi, T., Ogawa, A., Torigoe, S. and Saito, T. (2004). Micromechanics-based durability study of Polyvinyl Alcohol Engineered Cementitious Composite (PVA-ECC). *ACI Materials Journal*, **101,** 242-248.

Li, V.C., Lepech, M. and Li, M. (2005). *Field Demonstration of Durable Link Slabs for Jointless Bridge Decks Based on Strain-Hardening Cementitious Composites*. Michigan DOT report.

Li, V.C., Mishra, D.K. and Wu, H.C. (1995). Matrix Design for Pseudo Strain-Hardening Fiber Reinforced Cementitious Composites. *RILEM Journal of Materials and Structures*, **28,** 586-595.

Li, V.C., Wang, S. and Wu, C. (2001). Tensile Strain-hardening Behavior of PVA-ECC. *ACI Materials Journal,* **98,** 483-492.

Malhotra, V.M. (1970). Concrete ring for the determination of tensile strength of concrete.'' *ACI Materials Journal*,. **77,** 354–357.

Malhotra, V.M. (1980) *Strength and Freeze-Thaw Characteristics of Concrete Incorporating Granulated Blast-Furnace Slag.* CANMET, I.R., Energy, Mines & Resources, Ottawa, Canada, 79-38.

Malhotra, V.M. (1993). Fly Ash, Silica Fume and Rice- Husk Ash in Concrete. *A Review", Concrete International,* **15,** 23-28.

Manning, D.G. (1996). Corrosion performance of epoxy-coated reinforcing steel: North American experience. *Construction and Building Materials*, **10,** 349-365.

Maslehuddin, M., Saricimen, H. and Al-Mani, A. (1987). Effect of fly ash addition on the corrosion resisting characteristics of concrete. *ACI Materials Journal*, **84,** 42-50.

Marshall, D.B. and Cox, B.N. (1988). A J-integral method for calculating steady-state matrix cracking stresses in composites. *Mechanics of Materials*, **8,** 127–133.

Martys, N.S. and Ferraris, C.F. (1997). Capillary transport in mortars and concrete. *Cement and Concrete Research,* **27,** 747-760.

Maruta, M., Kanda, T., Nagai, S.and Yamamoto, Y. (2005). New high-rise RC structure using pre-cast ECC coupling beam. *Concrete Journal*, **43,** 18-26.

Mehta, P.K. (1985). Influence of Fly ash Characteristics on The Strength of Portland-Fly ash Mixtures. *Cement and Concrete Research*, 669-674.

Mehta, P.K. (1986). *Concrete: Structure, Properties, and Materials.* Prentice-Hall. Englewood Cliffs, New Jersey, pp. 353-367.

Mehta P.K. and Monteiro P.J.M. (2006). *Concrete: Structure, Properties, and Materials*. Third Edition, McGraw Hill, New York.

Mesbah, H.A. and Buyle-Bodin, F. (1999). Efficiency of polypropylene and metallic fibres on control of shrinkage and cracking of recycled aggregate mortars. *Construction and Building Materials,* **13**, 439–447.

Michigan Department of Transportation. (2001). *Michigan Test Method 111 - Determining an Aggregate Wear Index (AWI) By Wear Track Polishing Tests.* Michigan Department of Transportation, Lansing, Michigan.

Mihashi, H. and De Leite, J.P.B. (2004). State-of-the-art report on control of cracking in early age concrete. *Advanced Concrete Technology*, **2**, 141-154.

Miyazato, S. and Hiraishi, Y. (2005). *Transport properties and steel corrosion in ductile fiber reinforced cement composites*. Proceedings of the Eleventh International Conference on Fracture, Turin, Italy, March, pp. 20-25.

Moranville-Regourd, M. (1998). Cements Made From Blastfurnace Slag, *Lea's Chemistry of Cement and Concrete,* 4th Edition, P. C. Hewlett Ed., Arnold, London, pp. 663-674.

Mora, J., Aguado, A. and Gettu, R. (2003). The influence of shrinkage reducing admixtures on plastic shrinkage. *Materiales de Construccion*, **53**, 71-80.

Neville, A.M. (1996). *Properties of Concrete.* Fourth Edition, John Wiley & Sons, New York, pp. 884.

Oh, B.H., Cha, S.W., Jang, B.S. and Jang, S.Y. (2002). Development of high-performance concrete having high resistance to chloride penetration. *Elsevier Science SA, Nuclear Engineering and Design (Switzerland),* **212**, 221-231.

Qian, S. and Li, V.C. (2007). Simplified inverse method for determining the tensile strain capacity of strain hardening cementitious composites. *Journal of Advanced Concrete Technology,* **5,** 235–46.

Qian, S. and Li, V.C. (2008). Simplified inverse method for determining the tensile properties of strain hardening cementitious composites. *Journal of Advanced Concrete Technology,* **6,** 353–63.

Read, P., Carette, G.G. and Malhotra, V.M. (1990) *Strength Development Characteristics of High-Strength Concrete Incorporating Supplementary Cementing Materials*. High-Strength Concrete, Proceedings of the 2nd International Symposium, SP-121, Hester, W., ed., American Concrete Institute, Farmington Hills, Mich., 527-547.

Reinhardt, H.W. and Jooss, M. (2003) Permeability and self-healing of cracked concrete as a function of temperature and crack width. *Cement and Concrete Research*, **33,** 981-985.

Rokugo, K., Kunieda, M. and Lim, S.C. (2005). Patching repair with ECC on cracked concrete surface. *Proc. CONMAT 5*.

Rose, J.H. (1987). *The Effects of Cementitious Blast-Furnace Slag on Chloride Permeability of Concrete, Corrosion, Concrete, and Chlorides*. Malhotra, V. M. Ed., SP-102, American Concrete Institute, Detroit, 107-125.

Roy, D.M. (1992). *The Effect of Blast Furnace Slag and Related Materials on the Hydration and Durability of Concrete.* G. M. Idorn International Symposium, SP–131, J. Holm and M. Geiker, Eds., American Concrete Institute, Detroit, Michigan, pp. 195-208.

Sagues, A.A., Powers, R.G. and Locke, C.E. (1994). *Corrosion processes and field performance of epoxy-coated reinforcing steel in marine structures*. Corrosion 94, Houston, TX, pp.299.

Şahmaran, M. and Li, V.C. (2007). De-icing salt scaling resistance of mechanically loaded Engineered Cementitious Composites. *Cement and Concrete Research*, **37,** 1035-1046.

Şahmaran, M. and Li, V.C. (2008a). Influence of microcracking on water absorption and sorptivity of ECC. *Rilem Journal of Materials and Structures*, (in Press).

Şahmaran, M. and Li, V.C. (2008b). Durability of mechanically loaded Engineered Cementitious Composites under high alkaline environment. *Cement and Concrete Composites*, **30,** 72-81.

Şahmaran, M. and Li, V.C. (2009a). Durability Properties of Micro-Cracked ECC Containing High Volumes Fly Ash. *Cement and Concrete Research*, **39**, 1033-1043.

Şahmaran, M. and Li,V.C. (2009b). Influence of Microcracking on Water Absorption and Sorptivity of ECC. *RILEM-Journal of Materials and Structures*, **42**, 593-603.

Şahmaran, M., Lachemi, M., Hossain K.M.A. and Li, V.C. (2009). Internal Curing of Engineered Cementitious Composites for Prevention of Early Age Autogenous Shrinkage Cracking. *Cement and Concrete Research*, **39**, 893-901.

Şahmaran, M., Lachemi, M., Hossain, K.M.A., Ranade, R. and Li, V.C. (2009). Influence of Aggregate Type and Size on the Ductility and Mechanical Properties of Engineered Cementitious Composites. *ACI Materials Journal*, **106**, 308-316.

Şahmaran, M., Li, M. and Li, V.C. (2007). Transport properties of Engineered Cementitious Composites under chloride exposure. *ACI Materials Journal*, **104**, 604-611.

Şahmaran, M., Li, V.C. and Andrade, C. (2008). Corrosion resistance performance of steel-reinforced Engineered Cementitious Composites beams. *ACI Materials Journal*, **105**, 243-250.

Şahmaran, M., Li, V.C. and Li, M. (2007). Transport properties of Engineered Cementitious Composites under chloride exposure. *ACI Materials Journal*, **104**, 604-611.

Şahmaran, M., Yaman, İ. Ö. and Tokyay, M. (2007). Development of High Volume Low-Lime and High-Lime Fly-Ash-Incorporated Self Consolidating Concrete. *Magazine of Concrete Research,* **59**, 97-106.

Sakata, K., Kanda, T., Hiraishi, M. (2004). Application of direct sprayed ECC for retrofitting dam structure surface-application for Mitaka-Dam. *Japan Concrete Institute Concrete Journal*, **42**.

Sivasundaram, V., Carette, G.G. and Malhotra, V.M. (1990). Long term strength development of high-volume fly ash concrete. *Cement and Concrete Composites*, **12,** 263-270.

Soroushian, P., Nagi, M. and Hsu, J. (1992). Optimization of the use of lightweight aggregates in carbon fiber reinforced cement. *ACI Materials Journal*, **89**, 267-276.

Stang, H. and Li, V.C. (1999). *Extrusion of ECC-material*. In Proc. Of High Performance Fiber Reinforced Cement Composites 3 (HPFRCC 3) edited by H. Reinhardt and A. Naaman, Chapman & Hull, pp. 203-212.

Stark, J. and Ludwig, H.M. (1997). Influence of Water Quality on the Frost Resistance of Concrete. *Freeze-Thaw Durability of Concrete,* J. Marchand, M. Pigeon, and M. Setzer Eds.,E & FN Spon, London, pp. 157-164.

Suthiwarapirak, P., Matsumoto, T. and Kanda, T. (2002). Flexural fatigue failure characteristics of an Engineered Cementitious Composite and Polymer Cement Mortars. *Materials, Conc. Struc. Pavements*, **57**, 121-134.

Swamy, R.N. and Bouikni, Ammar. (1990). Some engineering properties of slag concrete as influenced by mix proportioning and curing. *ACI Material.Journal,* **87**.

Taguchi, G. (1985). *System of Experimental Design, Quality Resources*. New York, International Publications.

Tarun, R., Naik and Bruce, Ramme (1990). Effects of high-lime fly ash content on water demand, time of set and compressive strength of concrete. *ACI Materials Journal*, **87**, 619-626.

Taylor, H.F.W. (1997). *Cement Chemistry, Second Edition*. Thomas Telford Publishing, London, pp. 459

Tikalsky, P.J., Carrasquillo, P.M. and Carrasquillo, R.L. (1988). Strength and Durability Consideration Affecting Mix Proportioning of Concrete Containing Fly Ash in. *ACI Materials Journal,* **85**, 505-511.

Tuutti, K. (1982). Corrosion of steel in concrete. *CBI Swedish Cement and Concrete Research Institute*, Stockholm**, 100**, 159.

Wang, S. and Li, V.C. (2004). *Tailoring of pre-existing flaws in ECC matrix for saturated strain hardening*. Proceedings of FRAMCOS-5, Vail, Colorado, USA, pp. 1005–1012.

Wang, S. and Li, V.C. (2006). High-Early-Strength Engineered Cementitious Composites. *ACI Materials Journal,* **103**, 97-105.

Wang, S. and Li, V.C. (2007). Engineered Cementitious Composites with high-volume fly ash. *ACI Materials Journal*, **104**, 233–241.

Weimann, M.B.and Li, V.C. (2003). Hygral behavior of engineered cementitious composites (ECC). *International Journal for Restoration of Buildings and Monuments*, **9**, 513-534.

Weiss, W.J. and Shah, S.P. (2002). Restrained shrinkage cracking: the role of shrinkage reducing admixtures and specimen geometry. *Rilem Journal of Materials and Structures*, **35**, 85-91.

Wittmann, F.H. (2002). Crack formation and fracture energy of normal and high strength concrete. *Sadhana,* **27**, 413-423.

Yang, E. and Li, V.C. (2006). *A Micromechanical Model for Fiber Cement Optimization and Component Tailoring*. In: Proceedings of 10th International Inorganic-Bonded Fiber Composites Conference, San Paulo, Brazil, CD-Paper K4.

Yang, E.H., Yang, Y. and Li, V.C. (2007). Use of high volumes of fly ash to improve ECC mechanical properties and material greenness. *ACI Materials Journal*, **104**, 620-628.

Yang, Y., Lepech, M.D. and Li, V.C. (2005). Self-healing of ECC under cyclic wetting and drying. *Proceedings of Int'l Workshop on Durability of Reinforced Concrete under Combined Mechanical and Climatic Loads*, Qingdao, China, 231-242.

Zhang, J. and Li, V.C. (2002). Monotonic and fatigue performance in bending of fiber reinforced Engineered Cementitious Composite in overlay system. *Cement and Concrete Research*, **32**, 415-423.

Zhang, M.N. (1995). Microstructure, crack propagation, and mechanical properties of cement pastes containing high volumes of fly ashes. *Cement and Concrete Research*, **25**, 1165-1178.

Zhou, J., Qian, S., Beltran, M.G.M., Ye, G., VanBreugel, K. and Li, V.C. (2009). Development of Engineered Cementitious Composites with Limestone Powder and Blast Furnance Slag. *Rilem Journal of Materials and Structures*, **43**, 803-814.